

Review

Not peer-reviewed version

---

# Chiral Covalent Organic Frameworks for Enantioselective Fluorescence Sensing

---

[Li-Ke Wang](#)\*, [Xin-Ru Chen](#), [Tong-Yu Lin](#), [Yong-Liang Ban](#), [Zeng-Chen Liu](#), [Hua-Li Jia](#), [Hong Wang](#),  
[Yu-Bao Lan](#)\*

Posted Date: 23 April 2026

doi: 10.20944/preprints202604.1603.v1

Keywords: covalent organic frameworks; chirality; enantioselective fluorescence sensing; host-guest chemistry; turn-on fluorescence; enantioselective recognition



Preprints.org is a free multidisciplinary platform providing preprint service that is dedicated to making early versions of research outputs permanently available and citable. Preprints posted at Preprints.org appear in Web of Science, Crossref, Google Scholar, Scilit, Europe PMC.

Copyright: This open access article is published under a [Creative Commons CC BY 4.0 license](#), which permit the free download, distribution, and reuse, provided that the author and preprint are cited in any reuse.

Disclaimer/Publisher's Note: The statements, opinions, and data contained in all publications are solely those of the individual author(s) and contributor(s) and not of MDPI and/or the editor(s). MDPI and/or the editor(s) disclaim responsibility for any injury to people or property resulting from any ideas, methods, instructions, or products referred to in the content.

Review

# Chiral Covalent Organic Frameworks for Enantioselective Fluorescence Sensing

Li-Ke Wang <sup>1,\*</sup>, Xin-Ru Chen <sup>1</sup>, Tong-Yu Lin <sup>1</sup>, Yong-Liang Ban <sup>1</sup>, Zeng-Chen Liu <sup>1</sup>, Hua-Li Jia <sup>1</sup>, Hong Wang <sup>1</sup> and Yu-Bao Lan <sup>2,\*</sup>

<sup>1</sup> School of Chemistry and Chemical Engineering, Zhoukou Normal University, Zhoukou 466001, China

<sup>2</sup> Key Laboratory of Water Security and Water Environment Protection in Plateau Intersection (Ministry of Education), Key Laboratory of Bioelectrochemistry and Environmental Analysis of Gansu Province, College of Chemistry and Chemical Engineering, Northwest Normal University, Lanzhou 730070, P. R. China

\* Correspondence: wanglikebest@163.com (L.-K.W.); lanyb@nwnu.edu.cn (Y.-B.L.)

## Abstract

Chirality is a cornerstone of biological systems and pharmaceutical activity, driving a critical need for rapid and sensitive enantioselective analytical methods. Covalent organic frameworks (COFs) have emerged as versatile porous materials, and their chiral counterparts, chiral COFs (CCOFs), uniquely combine high surface area, predesignable pores, and a confined chiral microenvironment, making them exceptional platforms for enantioselective fluorescence sensing. This review systematically summarizes recent advances in the construction and application of CCOFs for enantioselective fluorescence sensing. We first outline the primary synthetic strategies for CCOFs, including direct synthesis, post-synthetic modification, and chiral induction. Subsequently, based on the direction of fluorescence signal change upon analyte binding, we classify the sensing mechanisms into three categories: “turn-off” (quenching via static complexation or photoinduced electron transfer), “turn-on” (enhancement through rigidification or suppression of electron transfer), and ratiometric (self-calibrating dual-emission response). Representative examples for the detection of amino acids, amino alcohols, terpenes, and saccharides are highlighted for each mode. Special emphasis is placed on structure–property relationships, such as the synergistic roles of hydrogen bonding,  $\pi$ – $\pi$  stacking, and framework confinement in amplifying enantioselectivity. Finally, we discuss current challenges and future perspectives, including the rational design of ratiometric sensors, integration into practical devices, and the convergence with machine learning to advance the field of smart chiral sensing.

**Keywords:** covalent organic frameworks; chirality; enantioselective fluorescence sensing; host-guest chemistry; turn-on fluorescence; enantioselective recognition

## 1. Introduction

Chirality is a fundamental geometric property that profoundly influences molecular interactions, playing a pivotal role in biological systems, pharmaceutical activity, and materials science [1–3]. The enantioselective recognition of chiral molecules is of paramount importance in diverse fields, including drug development, clinical diagnostics, agrochemical analysis, and food safety [4–6]. Conventional analytical techniques for chiral discrimination, such as high-performance liquid chromatography (HPLC) and capillary electrophoresis, often suffer from drawbacks like time-consuming procedures, high cost, and limited sensitivity [7,8]. Consequently, there is a growing demand for rapid, sensitive, and cost-effective enantioselective sensing platforms [9–13].

Fluorescence-based sensing has emerged as a powerful alternative due to its high sensitivity, fast response, operational simplicity, and real-time monitoring capability [14–16]. However, achieving enantioselective fluorescence discrimination remains challenging because of the subtle

physicochemical differences between enantiomers, which require exquisitely designed chiral microenvironments to amplify recognition events [17–19].

In recent years, covalent organic frameworks (COFs)—a class of crystalline porous polymers with pre-designable structures, high surface areas, tunable pore sizes, and excellent stability—have attracted tremendous interest in sensing applications [20–24]. Among them, chiral COFs (CCOFs) integrate the intrinsic advantages of COFs with chiral recognition elements, offering a unique platform for enantioselective fluorescence sensing [25–28]. The well-defined chiral nanochannels of CCOFs not only preconcentrate analytes but also provide confined spaces where host–guest interactions (e.g., hydrogen bonding,  $\pi$ – $\pi$  stacking, and electrostatic forces) are amplified, leading to significantly enhanced enantioselectivity compared to molecular analogs [29–34].

Despite rapid advances, the field of CCOF-based enantioselective fluorescence sensing is still in its early stages, with several key challenges remaining [27,35–37]: (i) the trade-off between crystallinity and chiral functionality during synthesis, (ii) the need for a deeper mechanistic understanding of signal transduction (turn-off vs. turn-on vs. ratiometric responses), (iii) limited analyte scope beyond model compounds, and (iv) the lack of practical device integration.

This review systematically summarizes the recent progress in the design, synthesis, and fluorescence sensing applications of CCOFs. We first introduce the three main synthetic strategies for constructing CCOFs. Then, we focus on their enantioselective fluorescence sensing mechanisms, categorizing them into turn-off (quenching), turn-on (enhancement), and ratiometric sensors, with representative examples for detecting amino acids, amino alcohols, terpenes, saccharides, and other chiral small molecules. Emphasis is placed on structure–property relationships, particularly how the confined chiral microenvironment amplifies enantioselectivity. Finally, we discuss current challenges and future perspectives, including rational design of ratiometric CCOF sensors, integration into portable devices, and convergence with machine learning for smart chiral sensing. By providing a comprehensive overview, this review aims to guide the rational development of next-generation CCOF-based enantioselective fluorescence sensors for practical applications in pharmaceutical, clinical, and environmental analysis, ultimately addressing the growing demand for rapid, sensitive, and selective chiral analysis.

## 2. Synthetic Strategies for CCOFs

The construction of CCOFs is the foundational step for their application in enantioselective fluorescence sensing. Without a well-defined crystalline porous architecture, the precise chiral microenvironment required for selective recognition cannot be established. A central challenge lies in introducing chirality without compromising the crystallinity and porosity that define CCOFs functionality—a delicate balance, as many chiral building blocks are bulky or flexible, hindering ordered stacking [25,29,38–40]. To date, three principal synthetic strategies have been established: (i) direct synthesis from enantiopure monomers [41–47], (ii) post-synthetic modification (PSM) of an achiral COF scaffold [48–51], and (iii) chiral induction from achiral precursors mediated by a chiral template or catalyst [52–57]. Each approach offers distinct advantages and trade-offs in terms of chiral site density, crystallinity retention, and synthetic accessibility.

### 2.1. Direct Synthesis

Direct synthesis involves the co-condensation of pre-designed chiral organic monomers into a crystalline framework [25]. This strategy ensures homogeneous distribution of chiral recognition sites throughout the COF skeleton and allows precise control over the chiral microenvironment [58–60]. However, it requires that the chiral monomers maintain conformational rigidity and do not sterically impede the reversible bond formation essential for crystallization. Based on the chiral source employed, current direct synthesis methods can be categorized into BINOL-based systems, camphorsulfonyl-based systems, tartaric acid-derived systems, and cyclodextrin-based systems [61–65].

**BINOL-Based CCOFs.** Optically pure 1,1'-bi-2-naphthol (BINOL) is one of the most versatile and widely used chiral sources in materials science due to its stable axial chirality and ease of functionalization [66,67]. Wu et al. reported BINOL-based fluorescent CCOFs by designing an enantiopure BINOL-dialdehyde monomer (BINOL-DA). Imine condensation with tetrakis(4-aminophenyl)ethene (TPE-TAM) or a triisopropyl-substituted triamine (iPr-TAM) yielded two 2D CCOFs (CCOF 7 and CCOF 8) with tetragonal and hexagonal pores, respectively (Figure 1a) [61]. The presence of twisted TPE units in CCOF 7 enabled facile exfoliation into ultrathin 2D nanosheets (7-NS), exposing abundant chiral recognition sites for vapor sensing. In a separate approach, Yuan et al. expanded the linkage chemistry by employing Knoevenagel polycondensation between a BINOL-22-crown-6-derived tetraaldehyde (BINOL<sup>2</sup>-C) and linear diacetonitriles. This afforded the first olefin (C=C) linked CCOFs (CCOF 17 and CCOF 18) [62]. Notably, these frameworks could be post-reduced via crystal-to-crystal transformation to yield C–C single bond-linked analogs (17-R and 18-R), demonstrating the chemical versatility of the olefin linkage.

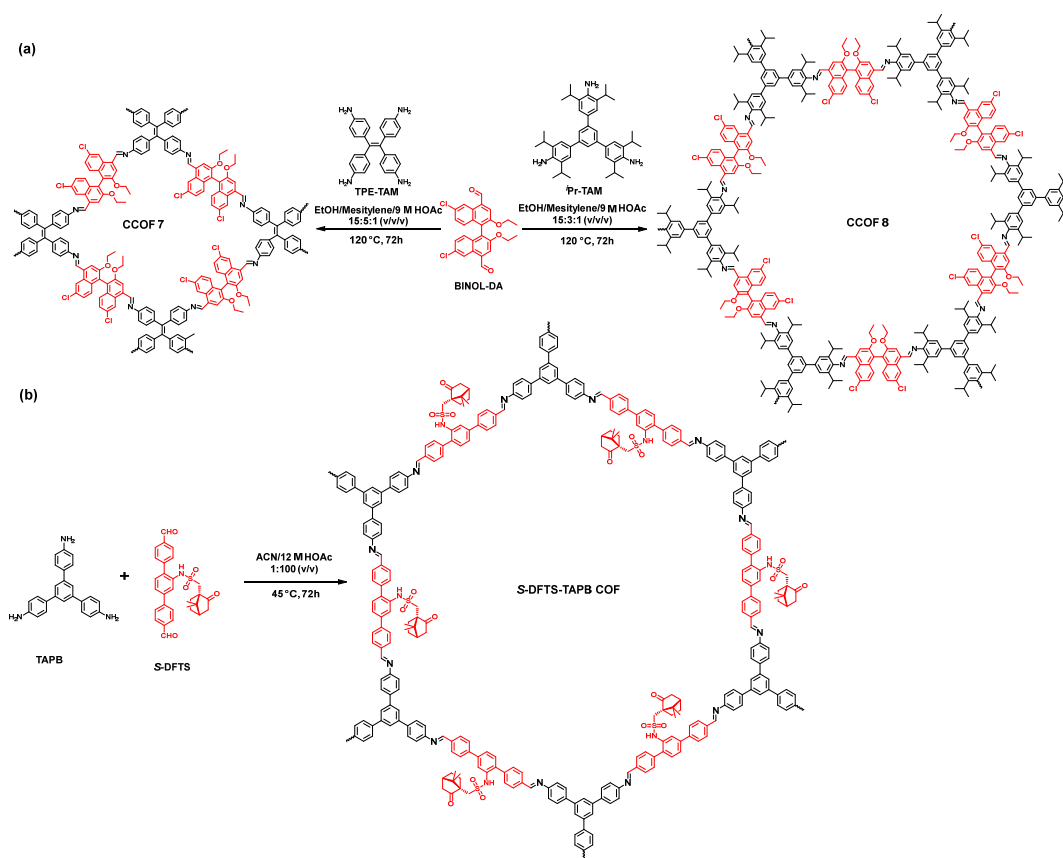


**Figure 1.** Synthesis of the CCOF 7 (a), CCOF 8 (a), and the (*R*)-DFST-TAPB COF (b) by direct synthesis.

**Camphorsulfonyl-Based CCOFs.** Moving beyond BINOL, Zhang et al. utilized (1*S*)-(+)-10-camphorsulfonyl chloride as a chiral source to synthesize a dialdehyde monomer (*S*-DFTS) bearing the camphorsulfonyl group. Schiff-base condensation with 1,3,5-tris(4-aminophenyl)benzene (TAPB) produced *S*-DFTS-TAPB COF (Figure 1b), which features 1D channels uniformly decorated with chiral camphorsulfonyl moieties [63]. The abundant hydrogen-bonding sites within these groups create a favorable microenvironment that enabled the CCOF-based enantioselective fluorescence sensing of non-aromatic amino acids—a significant breakthrough given the lack of  $\pi$ - $\pi$  interaction sites in such analytes.

**Tartaric Acid-Derived CCOFs.** Zhao et al. adopted a one-pot polymerization strategy using a chiral monomer (CTp) prepared by functionalizing 1,3,5-triformylphloroglucinol (Tp) with (+)-diacetyl-L-tartaric anhydride [64]. Condensation of CTp with 3,6-diaminocarbazole—a high-

efficiency fluorophore with a conjugated structure—yielded carbazole-conjugated chiral COFs (CC-COFs). The rigid triazine nodes and carbazole linkers endowed the material with a fluorescence quantum yield of 15.2% and a flower-like morphology, facilitating rapid and sensitive detection of phenylalanine enantiomers.

**Cyclodextrin-Based CCOFs.** Cyclodextrins (CDs) are naturally occurring chiral macrocycles that offer intrinsic host-guest recognition capabilities [68,69]. Han et al. leveraged this property by condensing  $\gamma$ -cyclodextrin ( $\gamma$ -CD) with trimethyl borate to yield an anionic CD-COF [65]. The inherent chirality of the  $\gamma$ -CD building blocks imparts optical activity to the entire framework. Subsequent cation exchange of the piperazinium counterions with  $Tb^{3+}$  afforded  $Tb@CD$ -COF, a dual-emission lanthanide-functionalized CCOF. The  $\gamma$ -CD cavities serve as enantioselective recognition pockets, while the incorporated  $Tb^{3+}$  ions provide a characteristic emission at 542 nm that responds to analyte binding via modulation of the antenna effect, enabling ratiometric sensing.

## 2.2. Post-Synthetic Modification

Post-synthetic modification circumvents the challenges associated with direct crystallization of chiral monomers by grafting chiral functionalities onto a pre-formed, highly crystalline achiral COF scaffold [25]. This strategy decouples framework construction from chiral functionalization: an achiral COF is first synthesized under optimized conditions to ensure high crystallinity and porosity, and chiral moieties are subsequently anchored to the pore walls through post-synthetic approaches [70–74].

**Quaternization on Ionic COFs.** Yue et al. synthesized an achiral ketoenamine-linked TB-COF via condensation of Tp and 2,2'-bipyridine-5,5'-diamine (BPY) under solvothermal conditions (Figure 2a) [75]. The framework features accessible pyridine units within its 1D channels. Subsequent quaternization with (1*R*,2*S*,5*R*)-2-isopropyl-5-methylcyclohexyl-carbonochloridate (*L*-MTE) in refluxing acetonitrile covalently anchored the chiral auxiliary to the pore walls, yielding *L*-TB-COF. PXRD confirmed the retention of crystallinity, while CD spectroscopy verified the successful introduction of chirality [76].

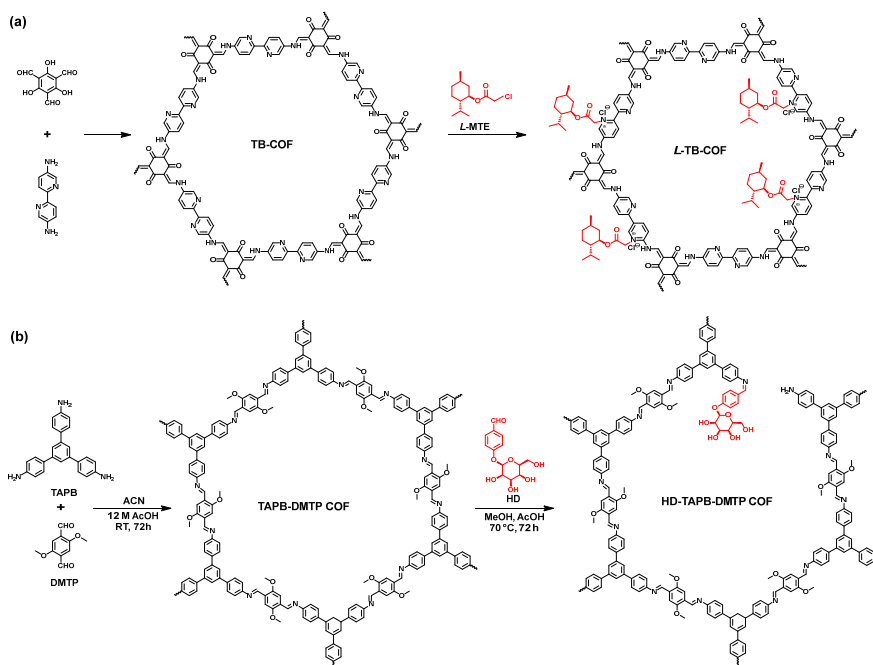


**Figure 2.** Synthesis of the *L*-TB-COF (a) and HD-TAPB-DMTP COF (b) via post-synthetic modification.

Chiral Monomer Exchange Strategy for Defective CCOFs. Yuan et al. employed a dynamic ligand exchange strategy. An achiral imine-linked TAPB-DMTP COF was first prepared from TAPB and 2,5-dimethoxyterephthaldehyde (DMTP) at room temperature (Figure 2b) [77]. The pre-formed COF was then treated with the chiral monodentate aldehyde helicid (HD) under acidic conditions, allowing partial exchange of DMTP with HD through dynamic imine bond cleavage and reformation. The resulting HD-TAPB-DMTP COF retained the imine-linked framework while acquiring chiral hydroxyl sites and structural defects.

### 2.3. Chiral Induction Synthesis

Chiral induction represents a fundamentally different paradigm: the crystallization of a homochiral framework from entirely achiral building blocks under the influence of a chiral or template catalyst [25]. This approach bypasses the need for synthetically complex or expensive chiral monomers, offering a cost-effective route to CCOFs [27].

Catalytic Induction with Chiral Amines. Han et al. pioneered this strategy for COFs by employing (*R*)- or (*S*)-1-phenylethylamine (1-PEA) as a chiral catalyst in the imine condensation of Tp with various diamines or triamines [52]. The chiral catalyst induced a unidirectional tilting of the threefold-symmetric tris(*N*-salicylideneamine) (TASN) cores, locking them into a propeller-like conformation of single handedness ( $\Lambda$  or  $\Delta$ ) throughout the crystallization process (Figure 3a). This yielded nine 2D CCOFs (TpPa-1, TpBD, TpTab, etc.) with controlled handedness from achiral precursors. Critically, the chiral catalyst was not incorporated into the final framework, as confirmed by  $^{13}\text{C}$  CP-MAS NMR and FT-IR spectroscopy.

Chiral Memory Effect in Cage-to-COF Transformation. Building on dynamic covalent chemistry (DCC), Song et al. discovered a “chiral memory” effect during the structural transformation from porous organic cages to COFs [55]. A homochiral imine cage (CC3-*R* or CC3-*S*), synthesized from achiral 1,3,5-triformylbenzene and chiral cyclohexanediamine, was subjected to linker exchange with various achiral diamines (Figure 3b). Remarkably, as the chiral linker was replaced, the propeller-like conformation of the benzene-1,3,5-methanimine cores was preserved, yielding 2D CCOFs with retained homochirality. This strategy effectively transfers chirality from a discrete cage to an extended framework without requiring any chiral monomers in the final product. Compared to direct catalytic induction, the cage-to-COF transformation offers greater control and ensures more complete preservation of chiral information.

Catalytic Asymmetric Polymerization. Expanding the scope of chiral induction beyond conformational locking, Chen et al. demonstrated that chiral phosphoric acid can catalyze an asymmetric multicomponent Povarov reaction to directly construct CCOFs with complex stereocenters [78]. Using (*R*)- or (*S*)-MCF-CPA as the chiral catalyst, achiral monomers—1,3,5-tris(4-formylphenyl)triazine (TFPT), 3-methyleneisoindolin-1-one (MIDO), and 1,3,5-tris(4-aminophenyl)triazine (TAPT)—were condensed under ambient conditions to yield C4-spiro-(2*S*, 4*R*)-TMTT-COF or C4-spiro-(2*R*, 4*S*)-TMTT-COF (Figure 3c). The resulting frameworks feature C4-azaspirocycle chiral centers—structural motifs ubiquitous in natural products and pharmaceuticals but unprecedented in COFs.

Each of the three synthetic strategies has its own advantages and trade-offs: direct synthesis offers the highest controllability and uniform distribution of chiral sites but requires rigid monomers; PSM retains the best crystallinity with mild conditions but has limited chiral loading capacity; chiral induction has the lowest cost and avoids chiral monomers, but its mechanism is complex and generalizability remains to be validated. Researchers should select the appropriate strategy based on the priorities of crystallinity, chiral density, and scalability for their target application.

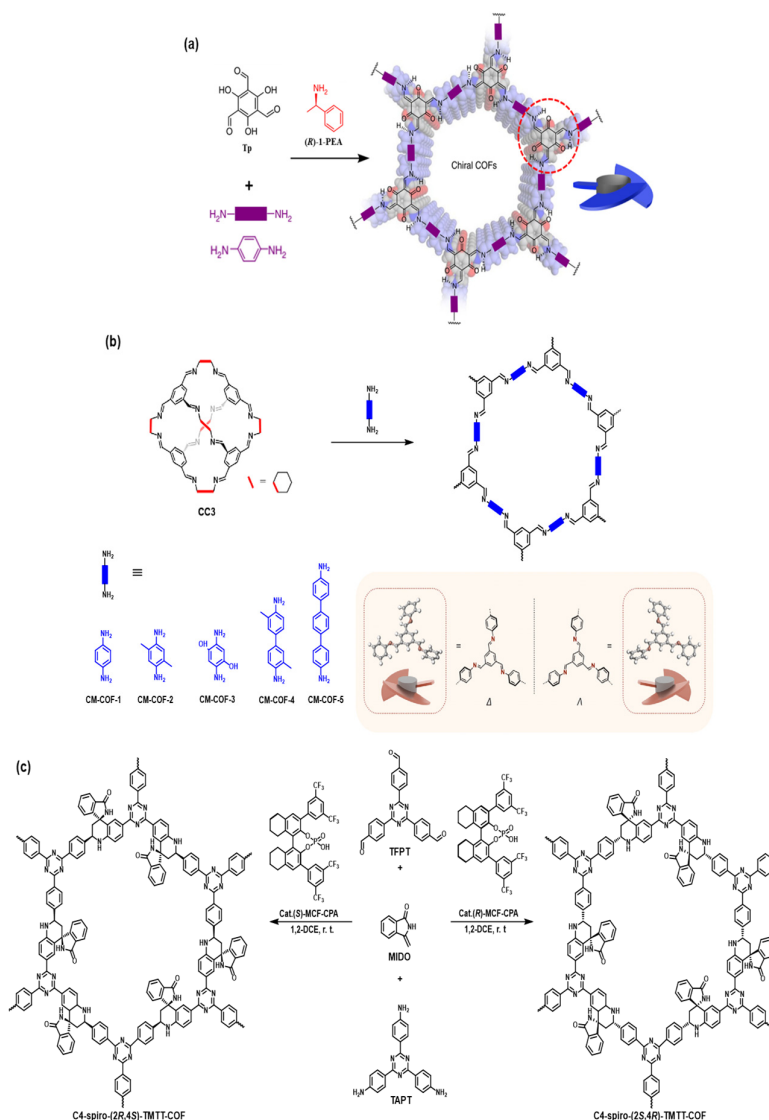


**Figure 3.** (a) Schematic representation of the synthesis of CCOFs by (R)-1-PEA. Adapted with permission from ref 52. Copyright 2018, Springer Nature. (b) Schematic representation of the synthesis of CM-COFs via cage-to-COF transformation. Adapted from ref. [55] with permission, copyright 2024, American Chemical Society. (c) Synthesis of C4-spiro-(2*S*, 4*R*)- and (2*R*, 4*S*)-TMTT-COFs via asymmetric multicompnent Povarov reaction.

### 3. Enantioselective Fluorescence Sensing of CCOFs

Fluorescence sensing is the extensively developed methodology for enantioselective recognition using CCOFs. The fundamental principle is that non-covalent interactions between target enantiomers and chiral fluorophores within the CCOF framework induce differential changes in photophysical properties, manifested as measurable variations in fluorescence intensity, wavelength, or lifetime [28,31,37,79–88]. The porous architecture of CCOFs amplifies these recognition events through analyte pre-concentration and the creation of well-defined chiral microenvironments[89]. Based on the direction of the fluorescence signal change upon analyte binding, CCOF-based enantioselective fluorescence sensors can be classified into three categories: turn-off (quenching), turn-on (enhancement), and ratiometric sensors [10,32,81]. To facilitate comparison across the three sensing modes, Table 1 summarizes representative CCOF-based fluorescence sensors along with their analytes, mechanisms, and enantioselectivity factors. In the following sections, we discuss

representative examples from each category, with an emphasis on the underlying recognition mechanisms and structure–property relationships.

**Table 1.** Representative CCOF-based fluorescence sensors for enantioselective recognition.

Signal Mode	CCOF Material	Analyte	Sensing Mechanism	Detection Limit	EF/QR	Ref.	
Turn-Off	TpTab ( $\Delta$ )	<i>D</i> -Cellobiose, <i>D</i> -Maltose, <i>D</i> -Glucose, <i>D</i> -Sucrose, <i>D</i> -Lactose, <i>D</i> -Sorbitol, <i>D</i> -Fructose, <i>D</i> -Gentiobiose, <i>D</i> -Lactobionic acid, <i>D</i> -Glucuronic acid, <i>D</i> -Gluconic acid, <i>D</i> -Mannitol	Static Quenching	N.R.	QR = 1.32–3.62	[52]	
		$\alpha$ -Pinene, Limonene, Fenchone, Carvone, Terpinen-4-ol			QR = 1.20–3.41		[61]
	7@PVDF membrane	$\alpha$ -Pinene, Limonene, Fenchone, Carvone, Terpinen-4-ol		N.R.	EF = 1.7–9.5	[61]	
	( <i>R</i> )-CCOF 17	<i>D</i> -Tryptophanol		PET-Promoted Quenching	N.R.	QR = 2.41	[62]
Turn-On	<i>L</i> -TB-COF	<i>R</i> -Phenylalaninol	Rigidification-Induced	0.8 $\mu$ M ( <i>R</i> )	EF = 16.96	[75]	
	C4-spiro-(2 <i>S</i> , 4 <i>R</i> )-TMTP-COF	<i>D</i> -Phenylalaninol		N.R.	EF = 25.39	[78]	
				12.5 $\mu$ M ( <i>D</i> )	EF = 7.25	[78]	
	(Δ)-CM-COF-3	<i>L</i> -Tyrosine, <i>L</i> -Phenylalanine		Rigidification-Induced	N.R.	EF = 16.28	[78]
					N.R.	EF = 2.19–2.24	[55]
	HD-TAPB-DMTP COF	<i>L</i> -Tyrosine, <i>L</i> -Phenylalanine			0.05–0.18 $\mu$ M ( <i>L</i> )	EF = 1.84–2.02	[77]
S-DFTS-TAPB COF	<i>D</i> -Arginine, <i>L</i> -Isoleucine, <i>L</i> -Valine		0.38–0.92 $\mu$ M	EF = 1.57–2.42	[63]		

	CC-COFs	<i>D</i> -Phenylalanine		0.027 $\mu$ M ( <i>D</i> )	N.R.	[64]
	( <i>R</i> )-CCOF 17	<i>L</i> -Phenylglycinol, <i>L</i> - Phenylalanine	PET- Suppressed Enhancement	N.R.	EF = 12.85– 14.72	[62]
Ratiometric	Tb@CD- COF	<i>R</i> -1,2-Propanediol, <i>R</i> -2- Amino-1-propanol, <i>R</i> -2- Amino-1-butanol	Antenna Effect- Modulated	7.5–11.8 $\mu$ M	$K_{BH}$ ratio = 1.25– 1.45	[65]

<sup>1</sup> Abbreviations: N.R. = Not reported; EF = Enantioselectivity factor; QR = Quenching ratio; PET = Photoinduced electron transfer; PAL = Phenylalaninol; PGL = Phenylglycinol; TPL = Tryptophanol; 7-NS = BINOL-based COF nanosheets; 7@PVDF = BINOL-based COF nanosheets embedded in PVDF nanofiber membrane.

### 3.1. Turn-Off (Quenching) Sensors

In turn-off sensors, the binding of chiral analytes leads to a decrease in fluorescence emission intensity. This quenching can arise from static complexation (formation of a non-emissive ground-state complex) or from dynamic processes such as photoinduced electron transfer (PET) that promote non-radiative decay [80,90–92]. Turn-off sensors have been successfully applied to the detection of saccharides, terpenes, and certain amino alcohol derivatives.

#### 3.1.1. Static Quenching via Host–Guest Complexation

Static quenching is characterized by unchanged fluorescence lifetime upon analyte binding, indicating the formation of a stable host–guest complex [31]. This mechanism is particularly effective for analytes that can engage in strong hydrogen bonding,  $\pi$ - $\pi$  stacking, or hydrophobic interactions within the confined chiral channels of the COF [52,61].

Saccharides. Han and co-workers employed a chiral induction strategy using (*R*)- or (*S*)-1-phenylethylamine as chiral catalysts to synthesize nine 2D CCOFs based on Tp [52]. Among these, TpTab—obtained from Tp and TAPB—exhibited strong fluorescence at 540 nm. In phosphate-buffered saline (pH 7.35) simulating human body fluids, TpTab showed selective quenching toward *D*-cellobiose: ( $\Delta$ )-TpTab gave a Stern–Volmer constant  $K_{sv}$  of 13,086  $M^{-1}$ , while ( $\Delta$ )-TpTab gave 3806  $M^{-1}$  (quenching ratio QR = 3.44) (Figure 4a-c). Notably, the sensor was enantioselective towards a wide range of saccharides, including *D*-glucose, *D*-sucrose, *D*-lactose, and *D*-maltose, with QR values ranging from 1.32 to 3.62. Fluorescence lifetimes remained nearly constant upon titration, and PXRD confirmed framework stability, indicating static quenching via host–guest adduct formation.

Terpenes. Wu and co-workers reported a CCOF-based enantioselective fluorescence sensor using BINOL-derived chiral COF nanosheets (7-NS), which were obtained by exfoliation of an imine-linked 2D COF (CCOF 7) [61]. In acetonitrile suspension, 7-NS showed strong emission at 380 nm that was quenched by both  $\alpha$ -pinene enantiomers, but (–)- $\alpha$ -pinene gave  $K_{sv} = 1348 M^{-1}$ , while (+)- $\alpha$ -pinene gave only 395  $M^{-1}$  (QR = 3.41) (Figure 4d). Similar selectivity was observed for limonene, fenchone, carvone, and terpinen-4-ol (QR = 1.20–3.41) (Figure 4e). To address the practical issues of aggregation and difficult recovery associated with powdered COFs, the authors electrospun 7-NS with PVDF into free-standing nanofiber membranes (7@PVDF), which exhibited an enantioselective fluorescence decrease ratio (EF) of 9.5 for  $\alpha$ -pinene vapour and could be regenerated by heating (Figure 4f). Control experiments with monomeric BINOL-dialdehyde showed no chiral discrimination, proving that the confinement and rigidity of the COF framework are essential for amplifying enantioselectivity. Molecular simulations revealed that (–)- $\alpha$ -pinene binds more strongly to the BINOL units (binding energy –21.92 vs. –18.63 kcal/mol) due to closer proximity of its double bonds and aliphatic groups to the chiral binaphthyl backbone. This work established two enduring

design principles—nanosheet exfoliation to expose active sites and membrane fabrication for recyclable sensing—that have since guided the development of CCOF-based sensors.

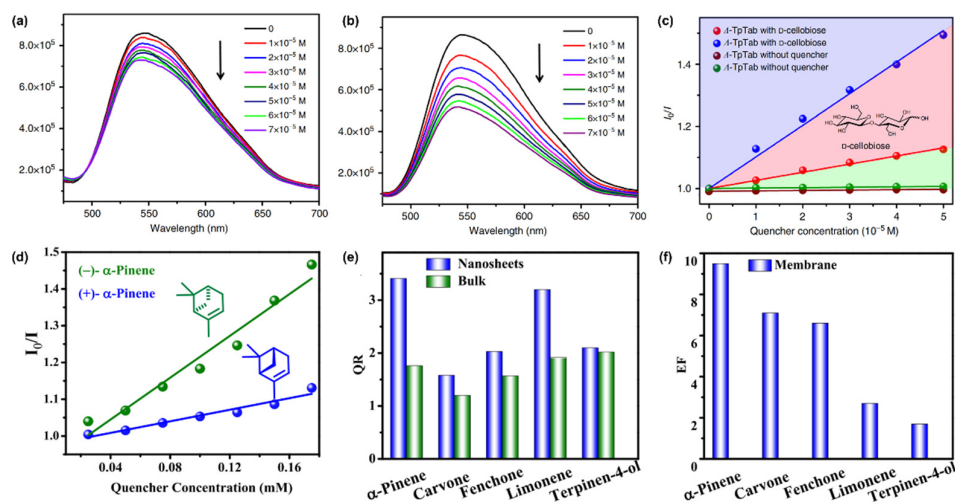


**Figure 4.** Fluorescence emission spectra of (Λ)-TpTab (a) and (Δ)-TpTab (b) with increasing concentration of the D-cellobiose quencher in solution. (c) Stern-Völmer plots of the fluorescence emissions of (Λ)/(Δ)-TpTab quenched by D-cellobiose. Adapted from ref. [52] with permission, copyright 2018, Springer Nature. (d) Stern-Völmer plots of 7-NS upon titration of α-pinene in MeCN. (e) Enantioselective quenching ratio for several terpenes. (f) Enantioselective fluorescence decrease ratio for several vapors. Adapted from ref. [61] with permission, copyright 2019, American Chemical Society.

### 3.1.2. PET-Promoted Quenching

While static quenching relies on ground-state complexation, an alternative quenching pathway involves photoinduced electron transfer (PET) that is facilitated upon analyte binding [93]. In this case, the analyte itself can act as an electron donor or acceptor, promoting non-radiative decay and enhancing quenching compared to the free COF [62].

Tryptophan. Yuan and co-workers synthesized olefin-linked chiral COFs (CCOFs 17 and 18) via Knoevenagel polycondensation of a chiral crown-ether-containing tetraaldehyde with diacetonitriles. When (R)-CCOF 17 was treated with tryptophan (TPL), the emission at 529 nm was quenched, with D-TPL ( $K_{sv} = 820.5 \text{ M}^{-1}$ ) quenching more efficiently than L-TPL ( $K_{sv} = 340.1 \text{ M}^{-1}$ ), giving a QR of 2.41 [62]. The indole ring of TPL is known to participate in  $\pi$ - $\pi$  stacking with the COF layers, which promotes PET from the excited fluorophore to the analyte, resulting in quenching. Interestingly, the same CCOF exhibited turn-on responses toward phenylglycinol and phenylalanine (discussed in Section 3.2.2), illustrating that the same material can produce opposite signal directions depending on the analyte's electronic properties and binding mode. This duality is a key insight: it suggests that the design of CCOF sensors must consider not only the chiral recognition site but also the electronic communication between the analyte and the fluorophore. For electron-rich analytes like TPL that can participate in  $\pi$ - $\pi$  stacking, PET-promoted quenching may dominate; for analytes that bind primarily through hydrogen bonding to the crown ether, PET suppression may lead to enhancement.

### 3.2. Turn-On (Enhancement) Sensors

In contrast to turn-off sensors, turn-on sensors exhibit an increase in fluorescence intensity upon analyte binding [80]. This enhancement typically results from the suppression of non-radiative decay pathways [94–97]. Two distinct sub-mechanisms have been identified: rigidification-induced enhancement, where analyte binding restricts molecular motions, and PET-suppressed enhancement,

where binding blocks an intrinsic electron transfer pathway [98–101]. In this section, we organize the discussion by analyte type within each sub-mechanism.

### 3.2.1. Rigidification-Induced Enhancement

When an analyte binds to a flexible fluorophore or to a COF with loose interlayer packing, it can lock the conformation and restrict motions that otherwise dissipate energy non-radiatively, thereby boosting fluorescence [31,102]. This is the most common turn-on mechanism reported for CCOFs, and it has been successfully applied to the detection of amino alcohols, aromatic amino acids, and non-aromatic amino acids[55,63,75,77,78].

**Amino Alcohols.** A representative example of rigidification-induced enhancement for amino alcohol detection is the chiral ionic COF developed by Yue and co-workers for phenylalaninol (PAL) [75]. They post-synthetically modified an achiral pyridine-based COF (TB-COF) with *L*-MTE via quaternization, producing the first chiral ionic COF used for fluorescence sensing. The material showed a remarkable turn-on response toward *R*-PAL:  $K_{BH} = 10,804 \text{ M}^{-1}$  for *R*-PAL versus only  $637 \text{ M}^{-1}$  for *S*-PAL (EF = 16.96), with detection limits of  $0.8 \text{ }\mu\text{M}$  (*R*) and  $13.2 \text{ }\mu\text{M}$  (*S*) (Figure 5a-c). *L*-TB-COF could also determine enantiomeric excess (*ee*) values with excellent linearity ( $R^2 = 0.9957$ ) over 10–100% *ee*. Neither free *L*-MTE nor achiral TB-COF showed any chiral recognition, demonstrating that anchoring the chiral moiety onto the rigid COF backbone is crucial. DFT calculations indicated that *R*-PAL forms stronger hydrogen bonds with ester oxygen atoms (binding energy  $-4.5 \text{ kcal/mol}$ ) than *S*-PAL ( $-0.2 \text{ kcal/mol}$ ) (Figure 5d). The exceptionally high EF value (16.96) suggests that the combination of ionic framework and hydrogen-bonding sites creates a uniquely well-defined chiral microenvironment (Figure 5e).

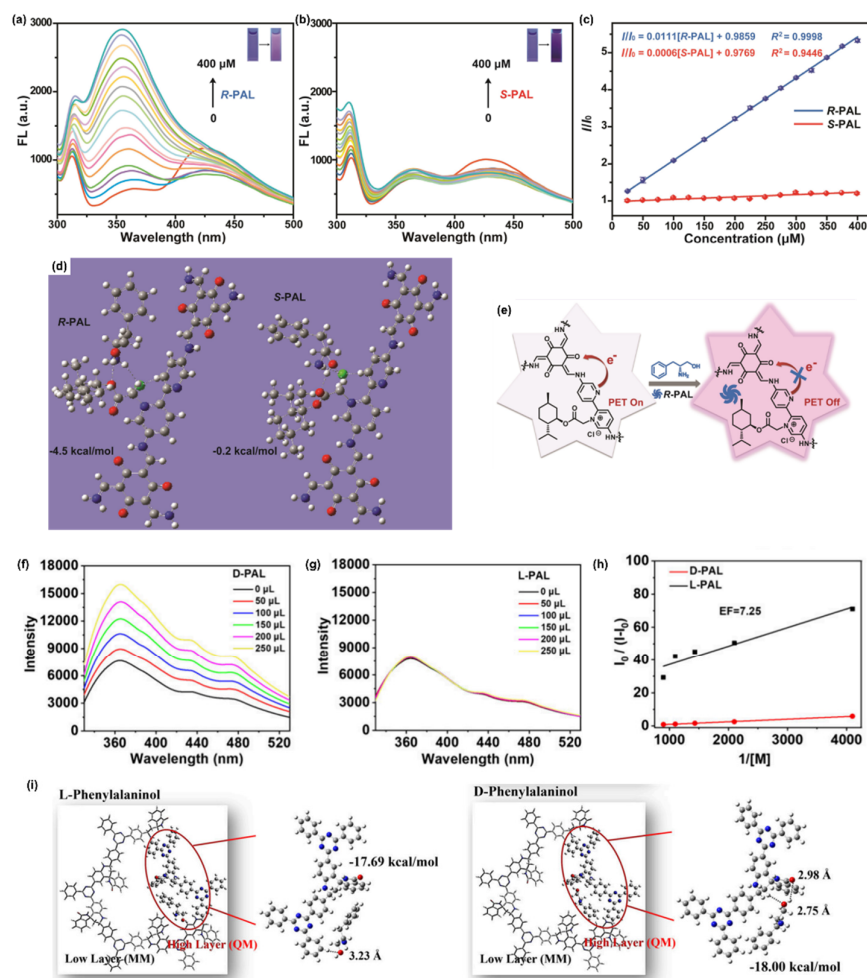


**Figure 5.** Fluorescence responses of *L*-TB-COF to *R*-PAL (a) and *S*-PAL (b) with different concentrations, and insets are the color change of the *R*-PAL detection system from 0 to 400  $\mu\text{M}$  under a UV lamp at 365 nm. (c) Linear calibration plots between  $I/I_0$  values of *L*-TB-COF and the concentrations of *R*-PAL (blue line) and *S*-PAL (red line). (d) Optimized structures of the most likely positions of *R*-PAL and *S*-PAL interacting with chiral fragments of *L*-TB-COF by DFT calculations (C, gray; O, red; N, blue; and H, white). (e) Proposed chiral fluorescent recognition mechanism. Adapted from ref. [75] with permission, copyright 2023, American Chemical Society. Fluorescence emission spectra of C4-spiro-(2*S*, 4*R*)-TMTT-COF in the presence of varying concentrations of *D*-PAL (f) and *L*-PAL (g) in suspension. (h) Benesi–Hildebrand plots of the fluorescence emissions of C4-spiro-(2*S*, 4*R*)-TMTT-COF enhanced by *D*-PAL and *L*-PAL in suspension. (i) Optimized structures of the possible positions of *D*-Phenylalaninol and *L*-Phenylalaninol interacting with single-layer chiral ring fragments of C4-spiro-(2*S*, 4*R*)-TMTT-COF by DFT calculations (C: gray; O: red; N: blue; H: white). Adapted from ref. [78] with permission, copyright 2025, American Chemical Society.

PAL has also been detected using C4-spirocyclic CCOFs reported by Chen and co-workers [78]. The resulting C4-spiro-(2*S*, 4*R*)-TMTT-COF contains two distinct carbon chiral centers and showed turn-on fluorescence toward *D*-PAL with  $K_{\text{BH}} = 641 \text{ M}^{-1}$  versus  $88 \text{ M}^{-1}$  for *L*-PAL (EF = 7.25), and a detection limit of 12.5  $\mu\text{M}$  for *D*-PAL (Figure 5f-h). By varying the monomers, C4-spiro-(2*S*, 4*R*)-TMTT-COF achieved an outstanding EF of 25.39 for PAL, one of the highest values reported. DFT calculations revealed that *D*-PAL formed more hydrogen bonds with the framework and had a more negative binding energy ( $-18.00$  vs.  $-17.69$  kcal/mol) than *L*-PAL (Figure 5i). The spirocyclic structure, with its rigid and well-defined three-dimensional geometry, appears to provide an exceptionally discriminating chiral environment.

**Aromatic Amino Acids.** Rigidification-induced enhancement has been extensively applied to the detection of tyrosine and phenylalanine. Song and co-workers exploited a chiral memory effect during dynamic covalent chemistry (DCC)-induced transformation from homochiral porous organic cages (CC3-R or CC3-S) to COFs—the first demonstration that chirality can be preserved during cage-to-COF transformation, yielding CCOFs constructed entirely from achiral building blocks. The resulting CM-COF-3, decorated with abundant hydroxyl groups, exhibited turn-on fluorescence toward *L*-tyrosine with  $K_{\text{BH}} = 1.16 \times 10^6 \text{ M}^{-1}$  versus  $5.18 \times 10^5 \text{ M}^{-1}$  for *D*-tyrosine (EF = 2.24) [55]. *L*-Phenylalanine was also recognized (EF = 2.19) (Figure 6a-c). DFT calculations using a three-layer COF model showed that *L*-tyrosine formed multiple hydrogen bonds (2.2–3.0 Å) with the pore walls, with a binding energy of  $-59.4$  kcal/mol, much more favourable than for *D*-tyrosine ( $-34.8$  kcal/mol) (Figure 6d).

A defective chiral COF approach was taken by Yuan and co-workers for the detection of tyrosine and phenylalanine [77]. They used a chiral monomer exchange strategy to introduce HD into an achiral TAPB-DMTP COF, yielding HD-TAPB-DMTP COF. In water, this material showed turn-on responses toward *L*-tyrosine (EF = 1.84; detection limits 0.18  $\mu\text{M}$  for *L* and 0.05  $\mu\text{M}$  for *D*) and *L*-phenylalanine (EF = 2.02; detection limits 0.17  $\mu\text{M}$  for *L* and 0.08  $\mu\text{M}$  for *D*) (Figure 6e-g). Molecular docking indicated that *L*-tyrosine formed four hydrogen bonds with the HD unit, whereas *D*-tyrosine formed only three (Figure 6h). The significantly lower detection limits for *D*-tyrosine (0.05  $\mu\text{M}$ ) compared to *L*-tyrosine (0.18  $\mu\text{M}$ ) suggest that the sensor is actually more sensitive to the non-preferred enantiomer—an unusual but potentially useful characteristic.

**Non-Aromatic Amino Acids.** The detection of non-aromatic amino acids—which lack  $\pi$ -conjugated systems and cannot engage in strong  $\pi$ - $\pi$  interactions with COF frameworks—is particularly challenging. Zhang and co-workers addressed this challenge by synthesizing *S*-DFTS-TAPB COF from (1*S*)-(+)-10-camphorsulfonyl chloride, achieving the first example of a CCOF-based fluorescent sensor for non-aromatic amino acids [63]. The material has camphorsulfonyl groups uniformly lining the 1D channels (pore size 3.6 nm, BET 445  $\text{m}^2/\text{g}$ ), creating a hydrogen-bond-rich chiral microenvironment. It exhibited turn-on fluorescence toward *D*-arginine (EF = 2.42; detection limits 0.68  $\mu\text{M}$  for *D* and 0.92  $\mu\text{M}$  for *L*) (Figure 7a-c). For isoleucine and valine, the *L*-isomers gave stronger enhancement (EF = 1.69 and 1.57, respectively). This reversal in enantioselectivity between



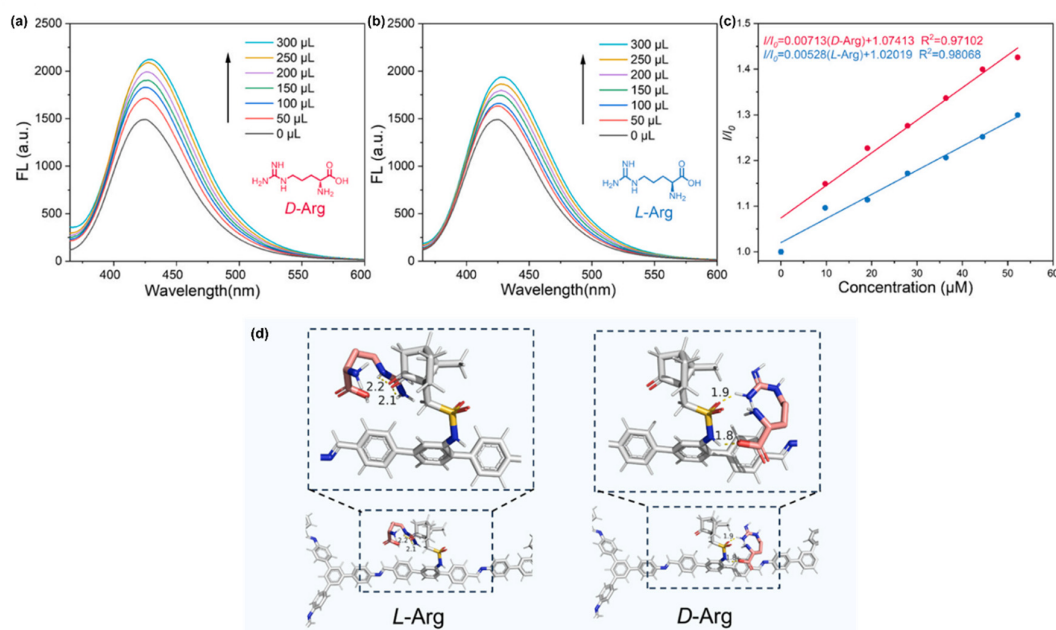


**Figure 7.** Fluorescence emission spectra with different concentrations of *D*-Arg (a) and *L*-Arg (b) linear. (c) Calibration plots between  $I/I_0$  values of S-DFTS-TAPB COF and the concentrations of *D*-Arg (red) and *L*-Arg (blue). (d) Schematic representation of the interaction of S-DFTS-TAPB with *D*-/*L*-Arg. Adapted from ref. [63] with permission, copyright 2026, ScienceDirect.

### 3.2.2. PET-Suppressed Enhancement

In the rigidification examples above, enhancement arises from physical restriction of motion. A conceptually different turn-on mechanism involves the suppression of an intrinsic PET pathway that normally quenches the fluorophore. When the analyte binds and blocks this electron transfer, fluorescence is restored [104–106]. This mechanism is common in systems where an electron-donating group and an electron-accepting group are both present in the COF, and it offers the advantage of typically producing larger signal changes because the initial “off” state has very low background fluorescence [107,108].

Phenylalanine. A representative example of PET-suppressed enhancement is the carbazole-conjugated CCOF developed by Zhao and co-workers for phenylalanine detection. They synthesized CC-COFs by one-pot polymerization of chiral (+)-diacetyl-*L*-tartaric anhydride-functionalized CTP with 3,6-diaminocarbazole. The carbazole group was selected for its high fluorescence efficiency and its ability to participate in PET. The material has a high quantum yield (15.2%) and showed turn-on fluorescence toward *D*-phenylalanine with detection limits of 0.027  $\mu\text{M}$  (*D*) and 0.037  $\mu\text{M}$  (*L*) over a linear range of 0.05–5  $\mu\text{M}$  [64]. These are among the lowest detection limits reported for CCOF-based sensors. Selectivity experiments confirmed that  $\pi$ - $\pi$  interactions with aromatic amino acids are essential for recognition—the sensor showed much weaker responses to aliphatic amino acids. The response was fast (80% within 10 min) and unaffected by ten common ions, indicating good practical potential (Figure 8a,b). The mechanism was attributed to inhibition of intramolecular PET from the carbazole donor to the methoxy acceptor upon analyte binding. This PET-based turn-on mechanism achieves very low detection limits because the initial fluorescence is low (due to efficient PET), and analyte binding produces a large relative enhancement—a “dark-to-bright” switching that is particularly advantageous for trace analysis.

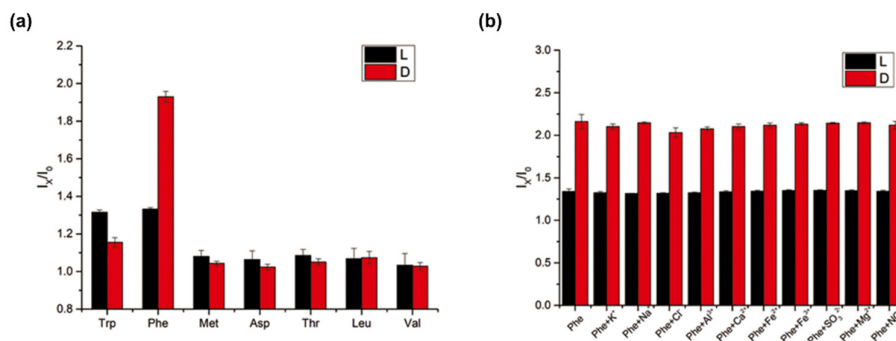


**Figure 8.** (a) Selectivity of CC-COFs to seven pairs of amino acid enantiomers. (b) The chiral recognition ability of CC-COFs for Phe enantiomers in interfering matrix. Adapted from ref. [64] with permission, copyright 2022, ScienceDirect.

Phenylglycinol and Phenylalanine. As mentioned in Section 3.1.2, the same (*R*)-CCOF 17 that quenched tryptophanol gave turn-on responses toward phenylglycinol (PGL) and PAL. For PGL,  $K_{BH}$  values were 2339  $M^{-1}$  for *L*-PGL and 159  $M^{-1}$  for *D*-PGL (EF = 14.72); for PAL, EF = 12.85 [62]. Mechanistically, the turn-on response is attributed to the binding of the protonated ammonium group of the analyte to the crown ether moiety, which suppresses photoinduced electron transfer (PET) from the crown ether oxygen atoms to the excited BINOL fluorophore. Strikingly, the homogeneous control experiment using the molecular analogue P-BINOL<sup>2</sup>-C—which lacks the COF framework—exhibited only weak quenching (Turn-off) towards these same analytes, with a quenching ratio (QR) of merely 1.28–1.30. This stark contrast, where the COF framework converts the molecular “turn-off” response into a “turn-on” one, highlights its critical role in creating a confined and ordered chiral microenvironment. Such confinement does more than just immobilize the chiral receptor; it fundamentally alters the photophysical pathway, likely by restricting non-radiative decay processes (e.g., through rigidification or modulating layer-stacking interactions), thereby amplifying the otherwise inefficient PET suppression observed in solution. Reduction of the olefin linkages to C–C single bonds (CCOFs 17-R and 18-R) produced blue-shifted emission and higher quantum yields but drastically reduced enantioselectivity (EF = 1.30–1.84), demonstrating that  $\pi$ -conjugation along the COF backbone is essential for efficient chiral information transfer. This trade-off between stability (of reduced frameworks) and sensitivity (of olefin-linked frameworks) is an important consideration for the design of future CCOF sensors.

### 3.3. Ratiometric Sensors

Ratiometric fluorescence sensors measure the intensity ratio at two different wavelengths, providing an internal reference that eliminates interference from variations in sensor concentration, excitation intensity, or environmental factors [82,109–111]. This self-calibrating feature is particularly valuable for quantitative analysis in complex samples [112,113].

Chiral Small Molecules. Han and co-workers prepared an anionic CD-COF from  $\gamma$ -cyclodextrin and trimethyl borate, then exchanged the piperazine counterions with  $Tb^{3+}$  to give  $Tb@CD$ -COF (Figure 9a) [65]. This design combines the chiral recognition ability of cyclodextrin with the luminescent properties of lanthanide ions. The material exhibits two distinct emission bands under excitation at 296 nm: a framework-based emission at 402 nm and a characteristic  $Tb^{3+}$  emission at 542 nm. The antenna effect from  $\gamma$ -CD to  $Tb^{3+}$  is intrinsically inefficient—the energy gap between the triplet state of  $\gamma$ -CD ( $2.17 \times 10^4 \text{ cm}^{-1}$ ) and the  $^5D_4$  level of  $Tb^{3+}$  ( $2.04 \times 10^4 \text{ cm}^{-1}$ ) is only  $1.3 \times 10^3 \text{ cm}^{-1}$ , below the threshold for efficient energy transfer ( $1.5 \times 10^3 \text{ cm}^{-1}$ ). As a result, the COF framework emission is partially quenched (“off” state). Upon addition of chiral analytes such as 1,2-propanediol, 2-amino-1-propanol, or 2-amino-1-butanol, the analytes compete with  $\gamma$ -CD for  $Tb^{3+}$  binding, weakening the  $Tb^{3+}$ – $\gamma$ -CD interaction (Figure 9b). This competitive  $\gamma$ -binding restores the COF emission at 402 nm

(“on” state) while simultaneously reducing the Tb<sup>3+</sup> emission at 542 nm. Consequently, the intensity ratio  $I_{402}/I_{542}$  changes monotonically with analyte concentration and enantiomeric configuration. The degree of recovery differs between enantiomers, yielding  $K_{BH}$  ratios (*R/S*) of 1.25–1.45 and detection limits of 7.5–11.8 μM. This work introduces a new paradigm for CCOF-based sensing: instead of relying on direct analyte–fluorophore interactions, the sensor uses an indirect “competitive binding” mechanism that decouples recognition from signal transduction (Figure 9c). The dual emission intrinsically enables ratiometric measurement, and future designs could exploit such dual-emission centers—via lanthanide doping or incorporation of reference fluorophores—to achieve robust, self-calibrating enantioselective detection, which is particularly advantageous for complex biological or environmental matrices. [114].

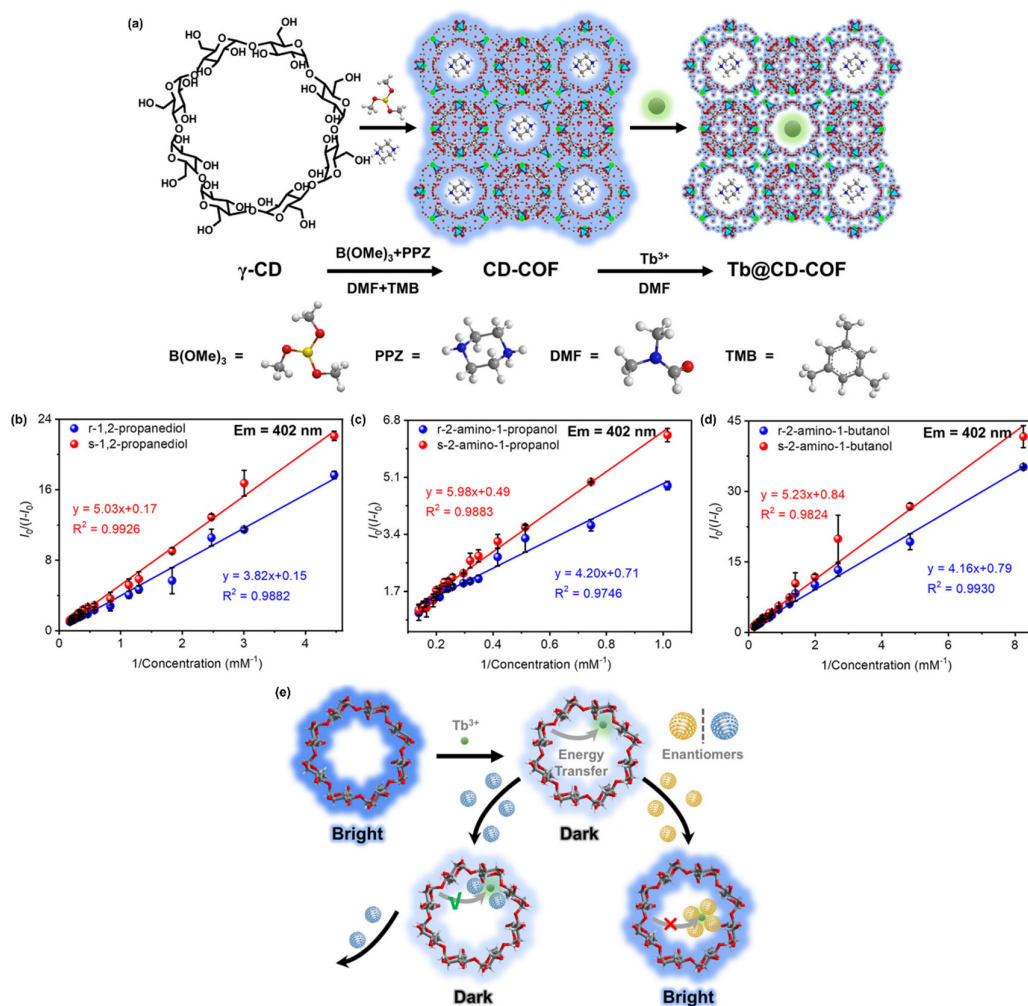


**Figure 9.** (a) The synthesis of Tb@CD-COF. Emission intensity changes of Tb@CD-COF towards 1,2-propanediol (b), 2-amino-1-propanol (c), and Tb@CD-COF (d) towards 2-amino-1-butanol at 402 nm. (e) Sensing mechanism of Tb@CD-COF towards enantiomers. Adapted from ref. [65] with permission, copyright 2025, Springer Nature.

#### 4. Conclusions and Future Perspectives

Remarkable progress has been made in the development of CCOFs for enantioselective fluorescence sensing. Three principal synthetic strategies have been established—direct synthesis, post-synthetic modification, and chiral induction—each offering distinct advantages in balancing crystallinity, porosity, and chiral functionality. In fluorescence sensing, CCOF-based sensors operate through three signal transduction modes: turn-off (quenching) via static complexation or

photoinduced electron transfer, achieving enantioselectivity factors up to 3.6 for terpenes and saccharides; turn-on (enhancement) via rigidification or PET suppression, dominating amino acid and amino alcohol detection with selectivity factors reaching 25.4; and ratiometric sensing, which remains nascent but has been demonstrated in dual-emission systems like Tb@CD-COF. The confined chiral nanochannels of CCOFs amplify enantioselectivity through analyte preconcentration and synergistic non-covalent interactions (hydrogen bonding,  $\pi$ - $\pi$  stacking, and electrostatic forces), with CCOFs consistently outperforming their molecular analogues—underscoring the essential role of framework confinement in chiral amplification.

Despite these advances, several challenges and opportunities remain.

First, expansion of the analyte scope. While aromatic and non-aromatic amino acids, amino alcohols, and terpenes have been successfully discriminated, application to more complex biomolecules (peptides, oligosaccharides, nucleic acids), chiral pharmaceuticals beyond model compounds, and environmentally relevant chiral pollutants (pesticides, herbicides) remains largely unexplored. The design of CCOFs with tailored recognition sites specifically for these challenging targets is a priority.

Second, deeper mechanistic understanding. Although DFT calculations and molecular docking have provided valuable insights, the dynamic nature of host-guest interactions within confined COF pores, the role of solvent effects, and cooperative binding phenomena remain poorly understood. Advanced in situ characterization techniques—solid-state NMR, time-resolved fluorescence microscopy, operando X-ray scattering—combined with theoretical models that account for framework flexibility and solvation, are urgently needed.

Third, rational material design for enhanced sensitivity and selectivity. Beyond the recent advances in structural innovation of CCOFs [115], the integration of multiple chiral recognition elements within a single COF framework, mimicking biological multivalency effects, could yield synergistic enhancements. Additionally, the deliberate design of ratiometric CCOF sensors—through lanthanide doping or incorporation of reference fluorophores—remains an important unmet goal [116–119].

Fourth, device integration and practical applications. Most reported sensors operate in suspension or as free-standing membranes. Translation into practical, user-friendly platforms requires fabrication of robust, reproducible, and cost-effective devices via inkjet printing, spin-coating, or in situ growth on electrodes. Integration with microfluidics, smartphone-based readout, and automated high-throughput screening would enable rapid on-site enantioselective analysis for pharmaceutical quality control, clinical diagnostics, and environmental monitoring.

Fifth, reusability and long-term stability. While CCOFs generally exhibit excellent chemical and thermal stability, the reversibility of the sensing process—essential for sensor regeneration and reuse—requires further optimization. Stimuli-responsive CCOFs that undergo reversible binding and release of chiral analytes in response to pH, temperature, or light represent an attractive approach for recyclable sensor systems.

Finally, convergence with emerging technologies. The combination of CCOF sensor arrays with machine learning algorithms could enable simultaneous discrimination of multiple chiral analytes [120–123]. Integration with optical fiber or waveguide platforms would facilitate remote and real-time sensing. Furthermore, leveraging the biocompatibility of certain CCOFs for chiral sensing in biological fluids and living systems could open new avenues for in vivo diagnostics and therapeutic monitoring [124–127].

In summary, the field of CCOFs for enantioselective fluorescence sensing has advanced remarkably over the past decade, establishing CCOFs as a powerful and versatile platform. With continued progress in synthetic methodology, mechanistic elucidation, and device engineering, CCOF-based fluorescence sensors hold great promise for addressing the growing demand for rapid, sensitive, and selective enantioselective analysis across pharmaceutical development, clinical diagnostics, and environmental monitoring. The convergence of CCOF chemistry with machine

learning, microfluidics, and nanophotonics is poised to drive the next generation of smart chiral sensing platforms, ultimately enabling real-world applications.

**Author Contributions:** Conceptualization, L.W. and Y.L.; writing—original draft preparation, L.W.; writing—review and editing, L.W. and Y.B.; visualization, X.C. T.L. H.J. and H.W.; supervision, L.W.; project administration, Z.L.; funding acquisition, L.W. and Y.L. All authors have read and agreed to the published version of the manuscript.

**Funding:** This research was funded the Henan Province Science Foundation for Youth (242300420581 and 252300420822), the Joint Fund for Science and Technology Research and Development Program of Henan Province (252103810108), and the Natural Science Foundation of Gansu Province (24JRRA132).

**Data Availability Statement:** No primary research results, software, or code have been included, and no fresh data were generated or analyzed as part of this review.

**Acknowledgments:** The authors have reviewed and edited the output and take full responsibility for the content of this publication.

**Conflicts of Interest:** The authors declare no conflicts of interest.

## Abbreviations

The following abbreviations are used in this manuscript:

COFs	Covalent Organic Frameworks
CCOFs	Chiral Covalent Organic Frameworks
HPLC	High-Performance Liquid Chromatography
PSM	Post-Synthetic Modification
BINOL	1,1'-bi-2-naphthol
TPE-TAM	Tetrakis(4-aminophenyl)ethene
Tp	1,3,5-triformylphloroglucinol
CD	Cyclodextrin
$\gamma$ -CD	$\gamma$ -Cyclodextrin
PET	Photoinduced Electron Transfer
TAPB	1,3,5-tris(4-aminophenyl)benzene
DMTP	2,5-Dimethoxyterephthaldehyde
HD	Helicid
DCC	Dynamic Covalent Chemistry
TASN	Tris(N-salicylideneamine)
1-PEA	1-Phenylethylamine
MIDO	3-Methyleneisoindolin-1-one
TAPT	1,3,5-Tris(4-aminophenyl)triazine
TFPT	1,3,5-Tris(4-formylphenyl)triazine
PAL	Phenylalaninol
PGL	Phenylglycinol
TPL	Tryptophanol
EF	Enantioselectivity Factor
QR	Quenching Ratio
ee	Enantiomeric Excess
DFT	Density Functional Theory
PVDF	Polyvinylidene Fluoride
7-NS	BINOL-based COF Nanosheets
BET	Brunauer–Emmett–Teller
PXRD	Powder X-ray Diffraction
FT-IR	Fourier Transform Infrared Spectroscopy
NMR	Nuclear Magnetic Resonance
CP-MAS	Cross-Polarization Magic Angle Spinning
CC	Carbazole-Conjugated
Tb@CD-COF	Terbium-exchanged Cyclodextrin COF

## References

1. Bada, J. L. Origins of homochirality. *Nature* **1995**, *374*, 594–595.
2. Board, E. Origins of Life and Evolution of Biospheres. *Origins Life Evol. Biosphere* **2010**, *35*, 75–77.
3. Yao, Y.; Ávalos-Ovando, O.; Ding, T.; Alvarez-Puebla, R. A.; Yu, P.; Ashalley, E.; Ma, L.; Wang, Z.; Markovich, G.; Govorov, A. O. From chiral biomolecules to chiral nanocrystals: A review of the latest developments and emerging concepts. *Chem* **2025**, *11*, 102544.
4. Kandula, J. S.; Rayala, V. P. K.; Pullapanthula, R. Chirality: An inescapable concept for the pharmaceutical, bio-pharmaceutical, food, and cosmetic industries. *Sep. Sci. Plus* **2023**, *6*, 2200131.
5. Bouz, G.; Žádny, J.; Storch, J.; Vacek, J. Chiral helical scaffolds: Unlocking their potential in biomolecular interactions and biomedical applications. *Biotechnol. Adv.* **2025**, *79*, 108513.
6. Chen, Z.; Chi, Z.; Sun, Y.; Lv, Z. Chirality in peptide-based materials: From chirality effects to potential applications. *Chirality* **2021**, *33*, 618–642.
7. Pieckowski, M.; Olędzka, I.; Bączek, T.; Kowalski, P. Deep Eutectic Solvents in Capillary Electromigration Techniques—A Review of Recent Advancements. *Molecules* **2025**, *30*, 3674.
8. Bernardo-Bermejo, S.; Adámez-Rodríguez, S.; Castro-Puyana, M.; Marina, M. L. Chiral analysis by capillary electromigration techniques. *Trends Anal. Chem.* **2025**, *189*, 118256.
9. Qiu, S.; Chen, G.-Y.; Qin, Y.-D.; Li, T.-T.; Yang, F.-Q. Recent Advance in Electrochemical Chiral Recognition Based on Biomaterials (2019–2024). *Molecules* **2025**, *30*, 3386.
10. Sharma, V.; Mishra, Akash K.; Mishra, Neeraj K.; Vinod Chiral Luminescent Sensor for Enantiomer Discrimination. *Chirality* **2025**, *37*, e70057.
11. Pan, Q.; Guan, H.; Xu, W.; Zhao, J.; Liu, Y.; Cui, L.; Zhou, J. Recent advance for enantio-recognition of chiral drugs sensing: Electrochemical, electrochemiluminescent and photoelectrochemical application. *Biosens. Bioelectron.* **2025**, *273*, 117141.
12. Wang, S.; Li, H.; Fan, S.; Chen, L.; Zhou, H.; Pérez-Juste, J.; Pastoriza-Santos, I.; Wong, K.-y.; Zheng, G. Chiral Plasmonic Sensors: Fundamentals and Emerging Applications. *Angew. Chem. Int. Ed.* **2025**, *64*, e202514816.
13. Zhang, X.; Yin, J.; Yoon, J. Recent Advances in Development of Chiral Fluorescent and Colorimetric Sensors. *Chem. Rev.* **2014**, *114*, 4918–4959.
14. Kashyap, N.; Kim, J.; Sharma, B. K.; Gogoi, P. Innovative Optical Chemosensors for Ions and Small Molecules. *ChemistrySelect* **2025**, *10*, e04895.
15. Penasa, R.; Licini, G.; Zonta, C. Advances in chiral analysis: from classical methods to emerging technologies. *Chem. Soc. Rev.* **2025**, *54*, 10940–10955.
16. Ding, S.-Y.; Dong, M.; Wang, Y.-W.; Chen, Y.-T.; Wang, H.-Z.; Su, C.-Y.; Wang, W. Thioether-Based Fluorescent Covalent Organic Framework for Selective Detection and Facile Removal of Mercury(II). *J. Am. Chem. Soc.* **2016**, *138*, 3031–3037.
17. Fan, Y.; Chen, M. Emerging frontiers in chiral metal–organic framework membranes: diverse synthesis techniques and applications. *Nanoscale* **2025**, *17*, 13076–13093.
18. Mejía-Salazar, J. R. Nanophotonic Strategies for Chiral Biosensing: Nanoparticles, Metasurfaces, Magneto-Optical, and Quantum Approaches. *Adv. Photonics Res.* **2026**, *7*, e202500242.
19. Zhang, Y.-X.; Zhang, F.-Q.; Peng, A.-P.; Jiang, T.; Meng, Y.-X.; Li, Y.; Gu, S.-X.; Zhu, Y.-Y. Enantioselective recognition of amino acids in water using emission-tunable chiral fluorescent probes. *Chin. Chem. Lett.* **2026**, *37*, 111500.
20. Geng, K.; He, T.; Liu, R.; Dalapati, S.; Tan, K. T.; Li, Z.; Tao, S.; Gong, Y.; Jiang, Q.; Jiang, D. Covalent Organic Frameworks: Design, Synthesis, and Functions. *Chem. Rev.* **2020**, *120*, 8814–8933.
21. Feng, X.; Ding, X.; Jiang, D. Covalent organic frameworks. *Chem. Soc. Rev.* **2012**, *41*, 6010–6022.
22. Côté, A. P.; Benin, A. I.; Ockwig, N. W.; O’Keeffe, M.; Matzger, A. J.; Yaghi, O. M. Porous, Crystalline, Covalent Organic Frameworks. *Science* **2005**, *310*, 1166–1170.
23. Ding, S.-Y.; Wang, W. Covalent organic frameworks (COFs): from design to applications. *Chem. Soc. Rev.* **2013**, *42*, 548–568.
24. Diercks, C. S.; Yaghi, O. M. The atom, the molecule, and the covalent organic framework. *Science* **2017**, *355*, eaal1585.

25. Han, X.; Yuan, C.; Hou, B.; Liu, L.; Li, H.; Liu, Y.; Cui, Y. Chiral covalent organic frameworks: design, synthesis and property. *Chem. Soc. Rev.* **2020**, *49*, 6248–6272.
26. Li, X.; Zhang, S.; Gao, J.; Wang, Z.; Yu, Q.; Zhao, Y.; Cheng, P.; Chen, Y.; Zhang, Z. The recent developments and applications of chiral covalent organic frameworks. *Sci. Sin. Chim.* **2019**, *49*, 662–671.
27. Kang, X.; Stephens, E. R.; Spector-Watts, B. M.; Li, Z.; Liu, Y.; Liu, L.; Cui, Y. Challenges and opportunities for chiral covalent organic frameworks. *Chem. Sci.* **2022**, *13*, 9811–9832.
28. Qin, Y.; Li, D.; Yao, T.; Ali, A.; Wu, J.; Yao, S. Covalent organic frameworks and related innovative materials in chiral separation and recognition. *Biomed. Chromatogr.* **2024**, *38*, e6008.
29. Wang, Y.; Zhang, Y.; Yu, C.; Yin, B. H.; Chen, Q.; Sun, S.-P.; Wang, X. Chiral Covalent Organic Frameworks as Promising Materials for Racemate Resolution. *ACS Appl. Polym. Mater.* **2024**, *6*, 8706–8720.
30. Hou, B.; Li, Z.; Kang, X.; Jiang, H.; Cui, Y. Recent Advances of Covalent Organic Frameworks for Chiral Separation. *Chem. Res. Chin. Univ.* **2022**, *38*, 350–355.
31. Skorjanc, T.; Shetty, D.; Valant, M. Covalent Organic Polymers and Frameworks for Fluorescence-Based Sensors. *ACS Sens.* **2021**, *6*, 1461–1481.
32. Chen, H.; Xia, L.; Li, G. Recent progress of chiral metal–organic frameworks in enantioselective separation and detection. *Microchim. Acta* **2024**, *191*, 640.
33. Han, Z.; Wang, K.-Y.; Wang, M.; Shi, W. Indirect Construction of Chiral Metal–Organic Frameworks for Enantioselective Luminescence Sensing. *Acc. Chem. Res.* **2025**, *58*, 625–634.
34. Yang, F.; Zhao, X.; Usman, K. A. S.; Jiang, D.; Razal, J. M.; Wang, J.; Tao, J.; Zhang, J. Engineering coaxial MXene@CNT fibers via wet-spinning for balanced mechanical, electrical, and electrochemical performance. *J. Energy Storage* **2025**, *137*, 118719.
35. Wei, N.-X.; Chen, T.; Gu, Z.-G.; Zhang, J. Chiral covalent–organic frameworks as a new class of circularly polarized luminescent materials. *Mater. Chem. Front.* **2026**, *10*, 8–20.
36. Wu, Q.; Yang, T.; Shi, J.; Jia, L.; Xie, B.; Lu, W.; Zhao, T.; Yu, C.; Mo, X.; Xie, W.; Sheng, J. Application of fluorescent covalent organic frameworks in gas sensors. *Nanoscale* **2026**, *18*, 6184–6202.
37. Xia, Y.-Q.; Jing, S.-M.; Chang, L.-M.; Gu, Z.-G.; Zhang, J. Luminescent covalent organic frameworks: Classification to optical applications. *Chin. J. Struct. Chem.* **2026**, *45*, 100731.
38. Liu, G.; Sheng, J.; Zhao, Y. Chiral covalent organic frameworks for asymmetric catalysis and chiral separation. *Sci. China Chem.* **2017**, *60*, 1015–1022.
39. Zhuo, S.; Zhang, X.; Luo, H.; Wang, X.; Ji, Y. The Application of Covalent Organic Frameworks for Chiral Chemistry. *Macromol. Rapid Commun.* **2020**, *41*, e2000404.
40. Liu, P.; Dai, W.; Shen, X.; Shen, X.; Zhao, Y.; Liu, J.-J. Recent Advances in the Utilization of Chiral Covalent Organic Frameworks for Asymmetric Photocatalysis. *Molecules* **2024**, *29*, 5006.
41. Xu, H.-S.; Ding, S.-Y.; An, W.-K.; Wu, H.; Wang, W. Constructing Crystalline Covalent Organic Frameworks from Chiral Building Blocks. *J. Am. Chem. Soc.* **2016**, *138*, 11489–11492.
42. Zhang, J.; Han, X.; Wu, X.; Liu, Y.; Cui, Y. Multivariate Chiral Covalent Organic Frameworks with Controlled Crystallinity and Stability for Asymmetric Catalysis. *J. Am. Chem. Soc.* **2017**, *139*, 8277–8285.
43. Wang, L. K.; Zhou, J. J.; Lan, Y. B.; Ding, S. Y.; Yu, W.; Wang, W. Divergent Synthesis of Chiral Covalent Organic Frameworks. *Angew. Chem. Int. Ed.* **2019**, *58*, 9443–9447.
44. Wang, X.; Han, X.; Zhang, J.; Wu, X.; Liu, Y.; Cui, Y. Homochiral 2D Porous Covalent Organic Frameworks for Heterogeneous Asymmetric Catalysis. *J. Am. Chem. Soc.* **2016**, *138*, 12332–12335.
45. Hou, B.; Han, X.; Xie, H.; Yuan, C.; Guo, Y.; Chen, X.; Tang, X.; Su, S.; Jiang, H.; Ye, Z.-M.; Kirlikovali, K. O.; Liu, Y.; Farha, O. K.; Cui, Y. Single-Crystal X-ray Structures of Homochiral Brønsted Acidic Covalent Organic Frameworks. *J. Am. Chem. Soc.* **2025**, *147*, 12127–12137.
46. Tang, X.; Liao, X.; Cai, X.; Wu, J.; Wu, X.; Zhang, Q.; Yan, Y.; Zheng, S.; Jiang, H.; Fan, J.; Cai, S.; Zhang, W.; Liu, Y. Self-Assembly of Helical Nanofibrous Chiral Covalent Organic Frameworks. *Angew. Chem. Int. Ed.* **2023**, *62*, e202216310.
47. Zhang, Y.-J.; Li, L.-H.; Feng, J.; Deng, X.; Sun, T.; Huang, J.-F.; Fan, Y.-Q.; Lan, Y.-B.; Wang, Z.-P.; Li, X.-M.; Liang, L.; Ding, S.-Y.; Ma, Y.-H.; Peng, Y.; Wang, W. Observation of Chiral Channels in Helical Covalent Organic Frameworks. *J. Am. Chem. Soc.* **2024**, *146*, 11450–11456.

48. Xu, H.; Chen, X.; Gao, J.; Lin, J.; Addicoat, M.; Irle, S.; Jiang, D. Catalytic covalent organic frameworks via pore surface engineering. *Chem. Commun.* **2014**, *50*, 1292–1294.
49. Xu, H.; Gao, J.; Jiang, D. Stable, crystalline, porous, covalent organic frameworks as a platform for chiral organocatalysts. *Nat. Chem.* **2015**, *7*, 905.
50. Zhang, Y.; Guo, J.; VanNatta, P.; Jiang, Y.; Phipps, J.; Roknuzzaman, R.; Rabaâ, H.; Tan, K.; AlShahrani, T.; Ma, S. Metal-Free Heterogeneous Asymmetric Hydrogenation of Olefins Promoted by Chiral Frustrated Lewis Pair Framework. *J. Am. Chem. Soc.* **2024**, *146*, 979–987.
51. Chen, M.; Zhang, J.; Liu, C.; Li, H.; Yang, H.; Feng, Y.; Zhang, B. Construction of Pyridine-Based Chiral Ionic Covalent Organic Frameworks as a Heterogeneous Catalyst for Promoting Asymmetric Henry Reactions. *Org. Lett.* **2021**, *23*, 1748–1752.
52. Han, X.; Zhang, J.; Huang, J.; Wu, X.; Yuan, D.; Liu, Y.; Cui, Y. Chiral induction in covalent organic frameworks. *Nat. Commun.* **2018**, *9*, 1294.
53. Wang, J. C.; Kan, X.; Shang, J. Y.; Qiao, H.; Dong, Y. B. Catalytic Asymmetric Synthesis of Chiral Covalent Organic Frameworks from Prochiral Monomers for Heterogeneous Asymmetric Catalysis. *J. Am. Chem. Soc.* **2020**, *142*, 16915–16920.
54. Li, F.; Kan, J. L.; Yao, B. J.; Dong, Y. B. Synthesis of Chiral Covalent Organic Frameworks via Asymmetric Organocatalysis for Heterogeneous Asymmetric Catalysis. *Angew. Chem. Int. Ed.* **2022**, *61*, e202115044.
55. Song, Q.; Yang, J.; Zheng, K.; Zhang, T.; Yuan, C.; Yuan, L.-M.; Hou, X. Chiral Memory in Dynamic Transformation from Porous Organic Cages to Covalent Organic Frameworks for Enantioselective Recognition. *J. Am. Chem. Soc.* **2024**, *146*, 7594–7604.
56. Ren, X.-R.; Kou, B.; Hao, Q.; Bertocchi, F.; Xu, Y.; Wang, L.; Zhao, Z.-L.; Chen, T.; Wan, L.-J.; Wang, D. Radial growth of twist-stacked covalent organic framework nanofibers. *Nat. Commun.* **2025**, *17*, 29.
57. Li, W.; Xu, H.; Zhang, H.; Chen, H.; Ke, S.; Guo, G.; Wei, F.; Fu, J.; Jing, C.; Cheng, J.; Liu, S. Enantiopure Dual-Helical Covalent Organic Framework Nanotubes Mediated by Supramolecular Assembly. *J. Am. Chem. Soc.* **2025**, *147*, 41320–41330.
58. Zhang, K.; Tang, X.; Yang, X.; Wu, J.; Guo, B.; Xiao, R.; Xie, Y.; Zheng, S.; Jiang, H.; Fan, J.; Zhang, W.; Liu, Y.; Cai, S. Raising the Asymmetric Catalytic Efficiency of Chiral Covalent Organic Frameworks by Tuning the Pore Environment. *ACS Appl. Mater. Interfaces* **2024**, *16*, 10661–10670.
59. He, T.; On, I. K. W.; Bi, S.; Huang, Z.; Guo, J.; Wang, Z.; Zhao, Y. Crystalline Olefin-Linked Chiral Covalent Organic Frameworks as a Platform for Asymmetric Catalysis. *Angew. Chem. Int. Ed.* **2024**, *63*, e202405769.
60. Zhou, J.; Bai, Y.; Qiu, Q.; Liu, S.; Qiu, H.; Zhang, X.; Zhao, H. Ex-situ EPR approach to explore the electrochemical behaviour of Arylboron-Linked conjugated microporous polymer cathode. *Chem. Eng. J.* **2023**, *452*, 139576.
61. Wu, X.; Han, X.; Xu, Q.; Liu, Y.; Yuan, C.; Yang, S.; Liu, Y.; Jiang, J.; Cui, Y. Chiral BINOL-Based Covalent Organic Frameworks for Enantioselective Sensing. *J. Am. Chem. Soc.* **2019**, *141*, 7081–7089.
62. Yuan, C.; Fu, S.; Yang, K.; Hou, B.; Liu, Y.; Jiang, J.; Cui, Y. Crystalline C–C and C=C Bond-Linked Chiral Covalent Organic Frameworks. *J. Am. Chem. Soc.* **2021**, *143*, 369–381.
63. Zhang, K.; Li, J.; Cai, D.; Tang, X.; Zheng, S.; Fan, J.; Zhang, Y.; Zhang, W.; Cai, S. Camphorsulfonyl-modified chiral covalent organic framework for enantioselective fluorescence sensing of non-aromatic amino acids. *Colloids Surf. A* **2026**, *734*, 139411.
64. Zhao, Y.; Liu, H.; Sun, B. Chiral induction in carbazole-conjugated covalent organic frameworks: A supersensitive fluorescence sensing platform for chiral recognition. *Sens. Actuators B* **2022**, *354*, 131253.
65. Han, Z.; Sun, T.; Cheng, P.; Shi, W. Cation-induced enhanced enantioselective recognition by a chiral covalent-organic framework. *Commun. Chem.* **2025**, *8*, 206.
66. Krajnc, M.; Niemeyer, J. BINOL as a chiral element in mechanically interlocked molecules. *Beilstein J. Org. Chem.* **2022**, *18*, 508–523.
67. Yu, Y.; Hu, Y.; Ning, C.; Shi, W.; Yang, A.; Zhao, Y.; Cao, Z.-Y.; Xu, Y.; Du, P. BINOL-Based Chiral Macrocycles and Cages. *Angew. Chem.* **2024**, *136*, e202407034.
68. Qiu, H.; Zhu, B.; Zhu, J.; Chen, S.; Ma, C.; Xiang, H.; Tong, S. Recent advances in application of cyclodextrin-based chiral materials for enantioseparation. *Trends Anal. Chem.* **2024**, *175*, 117708.

69. Lopez, E. C. R. Cyclodextrin Covalent-Organic Frameworks: Bridging Host-Guest Chemistry and Porous Materials for Diverse Applications. *Nano Hybrids Compos.* **2026**, *50*, 35–57.
70. Zhang, H.; Li, Q.; Weng, B.; Xiao, L.; Tian, Z.; Yang, J.; Liu, T.; Lai, F. Edge engineering of platinum nanoparticles via porphyrin-based ultrathin 2D metal-organic frameworks for enhanced photocatalytic hydrogen generation. *Chem. Eng. J.* **2022**, *442*, 136144.
71. Zhang, R.; Li, Y.; Yan, J.; Zeng, J.; Liu, Y.; Zhang, M.; Liu, P.; Huang, X.; Zhang, E.; Cheng, K.; Chen, J.; Sun, J. Surface modification of PVDF membranes with quaternized chitosan for selective separation of negatively charged polysaccharides – exemplified with heparin. *J. Environ. Chem. Eng.* **2023**, *11*, 110666.
72. Hu, J.; Li, Y.; Liu, X.; Dong, Y.; Wan, G.; Chen, Y.; Li, D.; Ma, H.; Du, X.; Fu, Y.; He, D.; Li, J. Robust Zn metal anode by a Ti3C2Tx MXene/acrylonitrile-butadiene-styrene terpolymer composite coating. *Chem. Eng. J.* **2025**, *510*, 161929.
73. Liu, J.; Wu, J.; Wang, N.; Tian, F.; Li, J. Surface reconstruction of BiSI nanorods for superb photocatalytic Cr(VI) reduction under near-infrared light irradiation. *Chem. Eng. J.* **2022**, *435*, 135152.
74. Wang, Q.; Xing, C.; Feng, M.; Yang, Y.; Pang, D.; Feng, X.; Zhang, Y.; Wang, B. Enzyme-Assisted Confined Synthesis of Metal Nanoparticles in Covalent Organic Frameworks for Efficient Enzyme-Metal Cascade Catalysis. *Angew. Chem. Int. Ed.* **2025**, *64*, e202509105.
75. Yue, J.-Y.; Song, L.-P.; Shi, Y.-H.; Zhang, L.; Pan, Z.-X.; Yang, P.; Ma, Y.; Tang, B. Chiral Ionic Covalent Organic Framework as an Enantioselective Fluorescent Sensor for Phenylalaninol Determination. *Anal. Chem.* **2023**, *95*, 11078–11084.
76. Yang, F.; Lv, K.; Zhao, X.; Kong, D.; Kong, N.; Luo, Z.; Tao, J.; Zhou, J.; Razal, J. M.; Zhang, J. Hierarchical heterostructures of MXene and mesoporous hollow carbon sphere for improved ion accessibility and rate performance. *Chem. Eng. J.* **2024**, *494*, 153246.
77. Yuan, L.; Tang, X.; Zhang, K.; Chen, H.; Yang, X.; Fan, J.; Xie, M.; Zheng, S.; Cai, S. Construction of a Defective Chiral Covalent Organic Framework for Fluorescence Recognition of Amino Acids. *Chem. Asian J.* **2024**, *19*, e202400753.
78. Chen, Z.; Liu, Z.-R.; Zhang, J.; Yang, W.-T.; Kan, J.-L.; Fan, J.; Li, W.-Y.; Wang, J.-C.; Dong, Y.-B. Construction of C4-Spirocyclic Chiral Covalent Organic Frameworks Via Asymmetric Multicomponent Povarov Reaction for Enantioselective Sensing. *J. Am. Chem. Soc.* **2025**, *147*, 11647–11653.
79. Bai, H.; Feng, C.; Guo, R.; Chen, Y.; Yuan, W.; Du, Y.; Feng, Y.; Liu, W.; Liu, K.; Guo, F.; Wang, J.; Chen, D.; Zhang, R. Wireless gas sensor based on monolayer Ti3C2Tx-modified GaN/CuO heterostructures for ultrafast and trace detection of NO2 gas. *Chem. Eng. J.* **2025**, *524*, 169751.
80. Mukhopadhyay, S.; Mondal, P.; Chattopadhyay, P. Covalent organic framework as fluorescent turn-on/off sensor and an account of operating sensing mechanism. *Inorg. Chim. Acta* **2023**, *546*, 121318.
81. Zhang, Y.; Li, C.; Jiang, M.; Liu, Y.; Sun, Z. Advancements and Prospects of Metal-Organic Framework-Based Fluorescent Sensors. *Biosensors* **2025**, *15*, 709.
82. Liu, Y.-s.; Xue, R.; Yan, B. Development and prospects of covalent organic framework-based ratiometric fluorescent sensors. *Coord. Chem. Rev.* **2025**, *523*, 216280.
83. Martínez-Periñán, E.; Martínez-Fernández, M.; Segura, J. L.; Lorenzo, E. Electrochemical (Bio)Sensors Based on Covalent Organic Frameworks (COFs). *Sensors* **2022**, *22*, 4758.
84. Fan, J.; Jiang, G.; Li, J.; Qi, J.; Nalumansi, H. S.; Wang, J.; Pi, F. Covalent organic frameworks (COFs)-based advanced sensors for detecting food contaminants: Design strategies and applications. *Microchem. J.* **2025**, *211*, 113096.
85. Zhen, D.; Liu, C.; Deng, Q.; Zhang, S.; Yuan, N.; Li, L.; Liu, Y. A review of covalent organic frameworks for metal ion fluorescence sensing. *Chin. Chem. Lett.* **2024**, *35*, 109249.
86. Long, B.; Liu, Q.; Zhang, Q.; Xing, Q.; Deng, L.; Qu, F.; Wang, L.; Ye, D.; Yuan, Z. Analysis and Study of Covalent Organic Frameworks in Electrochemical Sensors for Water Environment Pollutant Detection. *Small Struct.* **2025**, *6*, 2500138.
87. Yue, Y.; Ji, D.; Liu, Y.; Wei, D. Chemical Sensors Based on Covalent Organic Frameworks. *Chem. Eur. J.* **2024**, *30*, e202302474.

88. Yang, Y.; Zhang, C.; Cao, D.; Song, Y.; Chen, S.; Song, Y.; Wang, F.; Wang, G.; Yuan, Y. Design and preparation of fluorescent covalent organic frameworks for biological sensing. *Chem. Commun.* **2024**, *60*, 2605–2612.
89. Xu, K.; Huang, N. Recent Advances of Covalent Organic Frameworks in Chemical Sensing. *Chem. Res. Chin. Univ.* **2022**, *38*, 339–349.
90. Zhen, D.; Zhang, S.; Yang, A.; Li, L.; Cai, Q.; Grimes, C. A.; Liu, Y. A PEDOT enhanced covalent organic framework (COF) fluorescent probe for in vivo detection and imaging of Fe<sup>3+</sup>. *Int. J. Biol. Macromol.* **2024**, *259*, 129104.
91. Zuo, M.; Zha, X.; Jiang, Z.; Luo, M.; Yan, Z.; You, H.; Qing, X.; Xiong, Y.; Liu, Y.; Liu, L.; Li, Y.; Wang, W.; Li, M.; Wang, D. AIE-Driven Chiral Covalent Organic Frameworks for Solid-State Circularly Polarized Luminescence, Hydrochromism, and Water-Induced Chiroptical Enhancement. *Angew. Chem. Int. Ed.* **2025**, *64*, e202509454.
92. Ma, W.; Gu, Z.; Pan, G.; Li, C.; Zhu, Y.; Liu, Z.; Liu, L.; Guo, Y.; Xu, B.; Tian, W. Dual-Response Photofunctional Covalent Organic Framework for Acid Detection in Various Solutions. *Chemosensors* **2023**, *11*, 214.
93. Singh, A. R.; Mohan, B.; Raghav, N.; Sagar, Virender; Abhishek; Pombeiro, A. J. L. Understanding the mechanisms and applications of luminescent covalent organic frameworks (COFs) for multi-analyte sensing. *J. Mol. Struct.* **2025**, *1321*, 139945.
94. Wang, E.; Zhou, X.; Yuan, H.; Li, J.; Liu, X. Design and optimization of a Micro-structured fiber temperature sensor based on surface plasmon resonance. *Measurement* **2023**, *217*, 113085.
95. Tang, Y.; Zheng, M.; Xue, W.; Huang, H.; Zhang, G. Combined Skeleton and Spatial Rigidification of AIEgens in 2D Covalent Organic Frameworks for Boosted Fluorescence Emission and Sensing of Antibiotics. *ACS Appl. Mater. Interfaces* **2022**, *14*, 37853–37864.
96. Zhang, L.; Geng, W.; Ou, X.; He, S.; He, X.-H.; Li, W.; Jiao, Y.; Zhou, Y.; Li, C.; Chen, Y.; Du, W.; Cheng, Z.; Jin, Z.; Lam, J. W. Y.; Qian, J.; Tang, B. Z. Boosting the Brightness of Covalent Organic Frameworks by Integration of Dual-Docking Luminogens with Aggregation-Induced Emission Effect. *J. Am. Chem. Soc.* **2025**, *147*, 39999–40009.
97. Liu, M.; Cheng, Y.-Z.; Fu, Y.; Bi, S.; Ding, X.; Han, B.-H.; Xu, Q.; Zeng, G. Boosting Covalent Organic Framework Luminescence by Suppressing Nonradiative Pathways. *Chin. J. Chem.* **2025**, *43*, 633–640.
98. Guo, J.; Bi, S.; He, T.; Cheng, Y.; Wang, S.; Wang, Z.; Dong, X.; Zhao, Y.; Zhao, Z.; Tang, B. Z.; Zhao, Y. Dynamic manipulation of photoluminescence in two-dimensional covalent organic frameworks. *Nat. Photon.* **2026**, *20*, 392–403.
99. She, W.-Z.; Li, C.-H.; Li, R. S.; Ling, J.; Cao, Q. Construction of two-dimensional fluorescent covalent organic framework nanospheres for the detection and removal of tetracycline. *Sep. Purif. Technol.* **2024**, *330*, 125294.
100. Zhao, J.; Zhang, C.; Qiu, Z.; Zhang, Z.; Lin, X.; Huang, S.; Zhang, J.; Wu, J.; Liao, L.; Wang, R. Novel Europium-Grafted 3D Covalent Organic Framework for Selective and Sensitive Fluorescence-Enhanced Detection of Levofloxacin. *Sensors* **2025**, *25*, 2304.
101. Zhang, X.-M.; Bai, Y.-M.; Ai, L.-L.; Wu, F.-H.; Shan, W.-L.; Kang, Y.-S.; Luo, L.; Chen, K.; Xu, F. A Chiral Metal–Organic Framework Prepared on Large-Scale for Sensitive and Enantioselective Fluorescence Recognition. *Molecules* **2023**, *28*, 4593.
102. Liu, Q.; Li, L.; Wang, M.; Wang, M.; Lan, Y.; Li, F.; Hu, J.; Xiao, Y.; Guo, X.; Wang, D.; Gao, D. Fabrication of flexibility-rigidity alternately assembled solid-state luminescence covalent organic frameworks: application to rifampicin antibiotics detection and latent fingerprint recognition. *Microchim. Acta* **2025**, *192*, 598.
103. Liu, P.; Li, X.; Zhang, A.; Zhang, J.; Zhang, J. Slope surface crack sensor based on a single-mode fiber conjugate helical structure. *Opt. Laser Technol.* **2025**, *192*, 114128.
104. Xiu, J.; Zhang, N.; Li, C.; Salah, A.; Wang, G. Tetraphenylethylene-based covalent organic frameworks as fluorescent chemosensor for rapid sensitive recognition and selective “turn-on” fluorescence detection of trace-level Al<sup>3+</sup> ion. *Microporous Mesoporous Mater.* **2021**, *316*, 110979.
105. Li, C.-H.; She, W.-Z.; Liu, J.-Z.; Li, R. S.; Ling, J.; Cao, Q. Synthesis of nanoflower-shaped covalent organic framework fluorescent probe for sensitive detection of aluminum ions. *Colloids Surf. A* **2024**, *691*, 133841.

106. Fan, J.; Li, J.; Zhou, W.; Gao, H.; Lu, R.; Guo, H. An 'on-off-on' fluorescent switch based on a luminous covalent organic framework for the rapid and selective detection of glyphosate. *Luminescence* **2023**, *38*, 1729–1737.
107. Peng, Q. The flexible covalent organic frameworks with 2,3,5,6-tetramethyl-1,4-phenylene for detecting nitrophenols by fluorescence and uptaking iodine. *Inorg. Chem. Commun.* **2026**, *189*, 116644.
108. Li, C.; Xu, X.; Xing, J.; Wang, F.; Shi, Y.; Zhao, X.; Liu, J.; Yang, Y.; Zhao, Z. A fluorescent dual-emissions UiO-66-NH<sub>2</sub>@TpTt-COF core-shell composite for sensitive and optosmart sensing of tetracycline. *Appl. Surf. Sci.* **2023**, *616*, 156455.
109. Bigdeli, A.; Ghasemi, F.; Abbasi-Moayed, S.; Shahrajabian, M.; Fahimi-Kashani, N.; Jafarinejad, S.; Farahmand Nejad, M. A.; Hormozi-Nezhad, M. R. Ratiometric fluorescent nanoprobe for visual detection: Design principles and recent advances - A review. *Anal. Chim. Acta* **2019**, *1079*, 30–58.
110. Yan, J.; Liu, S.; Sun, D.; Peng, S.; Ming, Y.; Ostovan, A.; Song, Z.; You, J.; Li, J.; Fan, H. Molecularly Imprinted Ratiometric Fluorescent Sensors for Analysis of Pharmaceuticals and Biomarkers. *Sensors* **2024**, *24*, 7068.
111. Hu, S.-R.; Yang, C.-R.; Huang, Y.-F.; Huang, C.-C.; Chen, Y.-L.; Chang, H.-T. Ratiometric Fluorescence Probe of Vesicle-like Carbon Dots and Gold Clusters for Quantitation of Cholesterol. *Chemosensors* **2022**, *10*, 160.
112. Liu, S.; Yan, J.; Sun, D.; Peng, S.; Li, J.; Fan, H. Ternary-Emission Molecularly Imprinted Ratiometric Fluorescence Sensor and Kit for the Rapid and Visual Detection of Enrofloxacin. *Biosensors* **2025**, *15*, 226.
113. Wen, Y.; Sun, D.; Yu, J.; Qi, J.; Zhang, Z.; Song, Z.; Wang, X.; Liu, H.; Chen, L.; Li, J. Recent advances in molecular imprinting-based ratiometric fluorescence sensors. *Sci. Sin. Chim.* **2023**, *53*, 196–206.
114. Chen, D.; Hao, Z.; Li, X.; Tong, X. Enhancing the Measurement Sensitivity and Repeatability of Electrolyte-Insulator-Semiconductor Capacitor Sensor With Impedance Conversion. *IEEE Trans. Instrum. Meas.* **2023**, *72*, 1–7.
115. Fu, S.; Zhang, X.; Dong, J.; Liu, Y.; Cui, Y. Helical Chiral Covalent Organic Frameworks Enable Enantioselective Surface Wetting. *J. Am. Chem. Soc.* **2026**, *148*, 8982–8992.
116. Sun, L.; Li, X.; Li, J.; Zeng, Y.; Lu, S. Understanding Orbital Hybridizations of Nickel-Based Catalysts for Urea Electrooxidation: Opportunities and Challenges. *Energy Fuels* **2025**, *39*, 13969–13996.
117. Yin, L.; Li, Y.; Hu, Y.; Wang, J.; Xue, Y.; Duan, W.; He, Y.; Tang, S.; Fu, T. Energy-saving extractive distillation using salt-based DESs as an entrainer for separating 2-propanol and water mixture. *J. Water Process Eng.* **2025**, *72*, 107433.
118. Zeng, M.-h.; Yao, Q.-h.; Zheng, F.; Jin, J.-w.; Zhang, Y.-y.; Ye, T.-x.; Chen, X.-m.; Guo, Z.-y.; Chen, X. Mimicking chirality floralform heterostructure: A multivariate metal-based nanoparticles with highly charge transformation interface and multivariate recognition. *Sens. Actuators B* **2024**, *419*, 136379.
119. Yang, X.; Li, S.; Zhao, P.; Li, X.; Zhang, G.; Zhang, Z.; Han, P.; Zhao, Y.; Zhang, T.; Liu, F.; Zhang, C.; Zhang, Y.; Wang, H. Nano-molecular dual-dimensional collaborative sensor for chiral amino acid discrimination and mechanism insights. *Biosens. Bioelectron.* **2026**, *292*, 118093.
120. Abbas, K.; Hasan, M. K.; Abbasi, A.; Mokhtar, U. A.; Khan, A.; Abdullah, S. N. H. S.; Dong, S.; Islam, S.; Alboaneen, D.; Ahmed, F. R. A. Predicting the Future Popularity of Academic Publications Using Deep Learning by Considering It as Temporal Citation Networks. *IEEE Access* **2023**, *11*, 83052–83068.
121. Wan, Y.; Wei, Q.; Sun, H.; Wu, H.; Zhou, Y.; Bi, C.; Li, J.; Li, L.; Liu, B.; Wang, D.; Wang, X.; Wang, C.; Liu, W. Machine learning assisted biomimetic flexible SERS sensor from seashells for pesticide classification and concentration prediction. *Chem. Eng. J.* **2025**, *507*, 160813.
122. Liu, J.; Meng, X.; Hu, C.; Wang, S.; Tang, J.; Luo, K.; Lin, Z. Metal covalent organic frameworks-based multi-signal nanozymes sensor array with machine learning for the intelligent recognition of sulfur-containing metallic salts. *Sens. Actuators B* **2025**, *444*, 138426.
123. Benedetto, G.; Stolz, R. M.; Meng, Z.; Chan, J. Y. M.; Shehayeb, E. O.; Morrell, C. T.; Fabusola, G.; Elsaesser, N.; Simon, C. M.; Mirica, K. A. Conductive Covalent Organic Frameworks as Chemiresistive Sensor Arrays for the Detection and Differentiation of Gasotransmitters. *J. Am. Chem. Soc.* **2025**, *147*, 43438–43452.
124. Luo, W.; Pan, X.; Ren, C.; Wang, T.; Li, G.; Jin, L.; Zhang, D. Anti-swelling and ROS-scavenging nanofiber hydrogel to prevent postoperative abdominal adhesion. *Chem. Eng. J.* **2025**, *516*, 164202.

125. Cai, Z.; Luo, W.; Zhuang, H.; Ren, C.; Pan, X.; Xu, Y.; Wang, H.; Li, X.; Yuan, Y.; Zhu, R.; Zhan, X.; Jin, L.; Xu, G. Dual-layer drug release system based on ureteral stents inhibits the formation of ureteral stricture. *Chem. Eng. J.* **2023**, *471*, 144596.
126. Saha, P.; Skrodzki, D.; Aditya, T.; Moitra, P.; Alafeef, M.; Dighe, K.; Molinaro, M.; Hicks, S. D.; Pan, D. Tailored Anti-miR Decorated Covalent Organic Framework Enables Electrochemical Detection of Salivary miRNAs for Mild Traumatic Brain Injury. *Small* **2025**, *21*, 2412107.
127. Wang, D.; Liu, Z.; Li, H.; Liu, G.; Li, X.; Pan, M.; Wang, R. Robust Hydrogel Sensors Induced by Intermolecular Mechanical Interlocking of Covalent Organic Frameworks for Non-Invasive Health Monitoring. *Adv. Mater.* **2025**, *37*, e20271.

**Disclaimer/Publisher's Note:** The statements, opinions and data contained in all publications are solely those of the individual author(s) and contributor(s) and not of MDPI and/or the editor(s). MDPI and/or the editor(s) disclaim responsibility for any injury to people or property resulting from any ideas, methods, instructions or products referred to in the content.